RUBIES FROM MONG HSU

By Adolf Peretti, Karl Schmetzer, Heinz-Jürgen Bernhardt, and Fred Mouawad

Large quantities of rubies—both rough and faceted—from a commercially important new source in Myanmar (Burma) have been available on the Bangkok market since 1992. The ruby crystals from the Mong Hsu marble deposit have dipyramidal to barrel-shaped habits and reveal dark violet to almost black "cores" and red "rims." With heat treatment, which removes their blue color component, the cores become intense red. The rubies grew under varying conditions in complex growth sequences. The color distribution between cores and rims is related to a different incorporation of chromium and/or titanium during crystal growth. Gemological, microscopic, chemical, and spectroscopic properties presented here permit the separation of faceted Mong Hsu rubies from their synthetic and other natural counterparts. Problems arising from artificial fracture fillings are also addressed.

ABOUT THE AUTHORS

Dr. Peretti, formerly director of the Gübelin Gemmological Laboratory, is an independent gemological consultant residing in Adligenswil, near Lucerne, Switzerland. Dr. Schmetzer is a research scientist residing in Petershausen, near Munich, Germany. Dr. Bernhardt is a research scientist at the Insititut für Mineralogie of Ruhr-Universität, Bochum, Germany. Mr. Mouawad is a Graduate Gemologist and vice-president of the Mouawad Group of Companies, Geneva, Switzerland, currently at Harvard University Business School, Cambridge, Massachusetts.

See acknowedgments at the end of the article. Photos and photomicrographs are by the authors, unless otherwise noted. Magnifications refer to the power at which the photomicrograph was taken.

Gems & Gemology, Vol. 31, No. 1, pp. 2–26.

Since 1992, Mong Hsu has been a primary source of ruby available in Thailand (figure 1). Mong Hsu is a small town situated in northeastern Myanmar (formerly Burma) in Shan State, which borders Thailand, Laos, and China. Untreated samples from this new source typically consist of bicolored corundum, with dark violet to almost black sapphire cores and ruby rims (figure 2). With heat treatment, the violet cores can be converted to red. Large quantities of untreated corundum crystals are brought into Thailand at Mae Sai and, to a lesser extent, at Mae Hong Son (see figure 3). In 1993, about 200 buyers from Chantaburi (Thailand) were spending several million U.S. dollars a month on Mong Hsu rough in Mae Sai ("Special report: Mong Hsu . . .," 1993). Thus, the Mong Hsu ruby has become an important source of supply to the world market.

In September 1992, one of the authors (AP) joined a group of gemologists who traveled to Myanmar and Vietnam at the invitation of the Asian Institute of Gemmological Sciences (AIGS), Bangkok, to learn about the occurrences of rubies and sapphires in these countries (see Jobbins, 1992; Kammerling et al., 1994). During this trip, at the mid-year Emporium in Yangon (Rangoon), Myanmar, the Myanma Gems Enterprise (MGE) announced a new ruby deposit in the region of Mong Hsu, and showed the group a series of rough samples with violet cores and red outer layers (called rims here for simplicity). Six samples were submitted for further study to one of the authors (AP), who also took the opportunity to test some cut stones (including heat-treated samples without violet cores) from this new source. The untreated rough and heat-treated cut rubies examined during that visit were essentially identical to the material examined later for this study. According to information subsequently obtained in Bangkok, many Thai dealers were already buying Mong Hsu rubies (see "Burma's Mong Hsu mine rediscovered . . .," 1993).

By October 1992, large quantities of faceted material approximately 0.5–1 ct in size and of high-quality color saturation and transparency had also begun to appear on the European market. One of the first lots of this material (obtained from a dealer in Munich) was studied in detail by

Figure 1. Since 1991, the Mong Hsu area in northeastern Myanmar has produced large quantities of superb rubies. This suite contains 58.22 ct of Mong Hsu rubies (the largest is 2.62 ct). Courtesy of Mouawad Jewellers; photo by Wicky Tjerk.

one of the authors (KS). Seventy of the 74 cut stones in this lot were almost identical with respect to their gemological characteristics, and unlike material from any other known locality; of the remaining four stones, two had typical Mogok features and two were typical of Thai ruby. When it was determined that the features of this new material were very similar to those of the Mong Hsu stones acquired in Yangon (notwithstanding any potential change of color and other properties that might be caused by heat treatment), the decision was made to carry out a complete study of these rubies.

Preliminary reports about some of the properties of Mong Hsu rubies have appeared in trade journals (Clark, 1993; Laughter, 1993a and b; Peretti, 1993; Milisenda and Henn, 1994), and an initial research study was published by Smith and Surdez (1994).

LOCATION

Although, because of security concerns, the authors were not able to visit the Mong Hsu deposit, first-hand information and photographs were obtained from miners in the summer of 1993. Reports on the local geology and mining operations have been published by Hlaing (1991, 1993, 1994) and are summarized below.

Mong Hsu is located about 250 km (150 miles) southeast of Mogok (figure 3), at an elevation of 700 m above sea level. It can be reached from Taung Gyi, the capital of Shan State, by traveling over a rough road for about 14 hours (Hlaing, 1994). Secondary (alluvial) corundum deposits are found in the terraces of Nam Hsu River, southeast of Mong Hsu township. These river terraces, where the first rubies were discovered and where mining and prospecting started, are 4 km long and 0.8 km wide, trending from northwest to southeast, and 80–160 m deep. In 1992, about 2,000 miners were working these alluvial deposits.

Additional secondary deposits have been found 16 km (10 miles) farther southeast. These extend over an area more than 100 km^2 between the two mountains Hsan Tao and Loi Paning. The "government

Figure 2. A distinctive feature of Mong Hsu ruby crystals is their deep violet (sapphire) core, which is surrounded by a red (ruby) rim. With heat treatment, the violet core becomes a deep red. This Mong Hsu ruby "thin section" is 5.3 mm wide; photo courtesy of John Emmett.

prospecting area" is restricted to a central 0.8 km^2 portion (figure 3). By 1994, about 500 joint ventures between private individuals and the Myanmar government were operating in the region (Hlaing, 1994), literally chewing up the surrounding hills (figure 4). Alluvial ruby is also found at Loi Khan and Mong Sang, which lie southwest and south (respectively) of Mong Hsu (again, see figure 3).

GEOLOGY AND MINERAL ASSEMBLAGES

According to the geologic map of Myanmar (Earth Sciences Research Division, 1977), the Mong Hsu ruby deposits are situated at the contact of upper Paleozoic marbles and other Paleozoic rocks, including various types of metamorphosed sediments. Hlaing (1991, 1993, 1994) reports that the major rock types in the region of the primary ruby occurrences are mica schist, phyllite, and calcsilicate rocks; the rubies occur in a marble belonging to this Paleozoic series.

Additional information on the different rock types in the vicinity of the Mong Hsu mines was obtained from the study of minerals that appear mixed with the ruby rough from the market at Mae Sai and on the surface of the corundum crystals themselves. These were identified by means of X-ray powder diffraction analysis, quantitative electron microprobe analysis, and a scanning electron microscope with energy-dispersive X-ray detector.

Figure 3. This map of the Mong Hsu region in northeastern Myanmar (see inset) shows the areas of current mining activity. The alluvial deposits (stippled areas), where the first rubies were found, are in river terraces southeast of the town of Mong Hsu. Primary occurrences of ruby with adjacent secondary deposits were discovered around Loi Hsan Tao . The pink region represents the area of gem potential suggested by prospecting in 1993. Adapted from Hlaing, 1993; courtesy of the Australian Gemmologist.

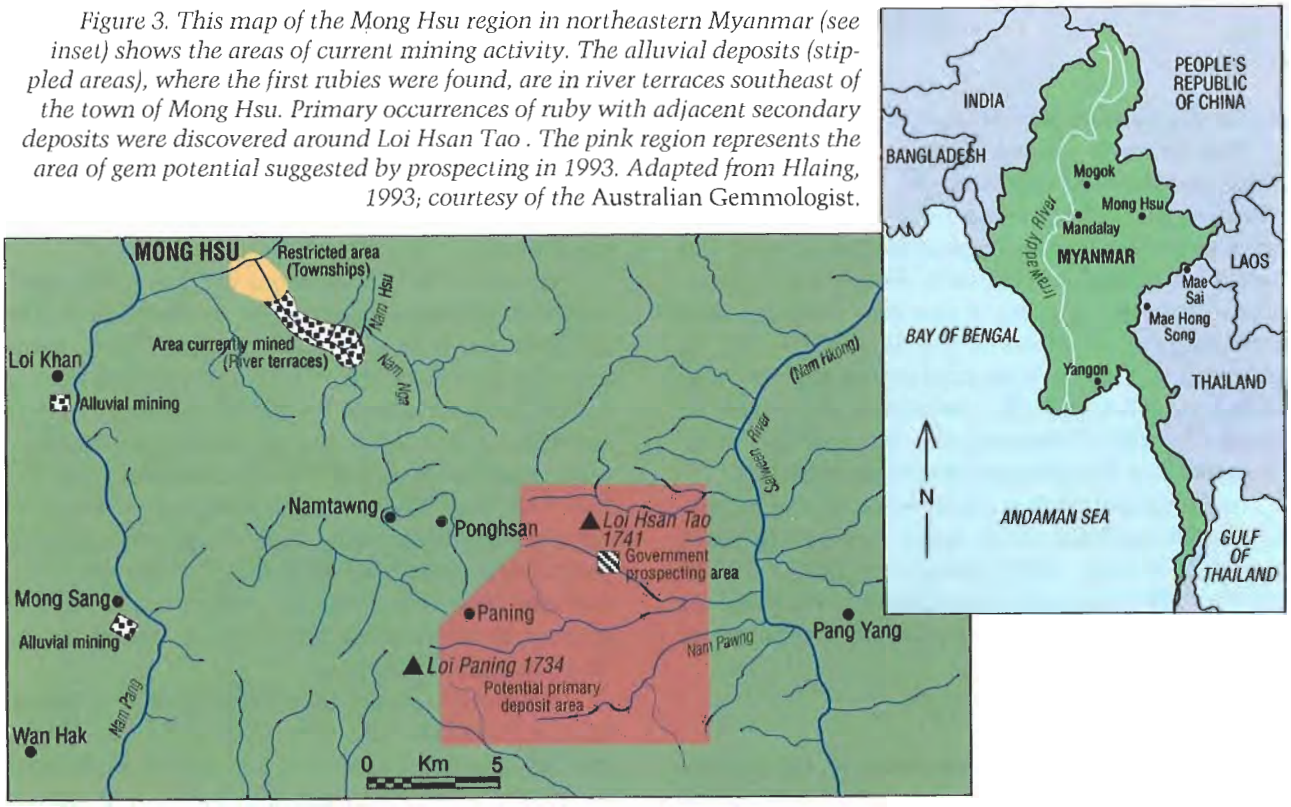

They include green and brown chromium-bearing dravite (tourmaline), andalusite, almandine, quartz, and green, chromium- and vanadium-bearing tremolite. One of the almandine crystals was overgrown with white mica. Overgrowths on the ruby crystals were identified as fuchsite (green mica), white mica, and light green Mg-chlorite.

Garnet, green tourmaline, tremolite, white mica, and quartz were also described by Hlaing (1993), with staurolite and pyrite mentioned as accessory minerals. The overgrowth of green tourmaline on Mong Hsu rubies noted by Hlaing (1993) was not found in this study; rather, all light green to green overgrowths on rubies available to us were identified as either fuchsite or Mg-chlorite.

From these mineral assemblages, it is evident that, although both the Mong Hsu and Mogok occurrences are metamorphic, they differ in the specific environment in which the rubies formed (Earth Sciences Research Division, 1977; Hlaing, 1981; Keller, 1983; Hunstiger, 1990; Kane and Kammerling, 1992; Kammerling et al., 1994). At Mogok, ruby occurs *in situ* in amphibolite-to-granulite facies metamorphosed marbles and calcsilicate marbles. In contrast, the mineral assemblages of Mong Hsu indicate marbles and metapelitic rocks metamorphosed to (lower temperature) amphibolite facies. Thus, Mogok represents a higher degree of metamorphism than does the Mong Hsu mining area.

MINING

Mining of the secondary deposits is by the classic methods used in Mogok (as described by, e.g., Kane and Kammerling, 1992) and elsewhere in Southeast Asia. In fact, a Mogok miner is believed to have been the first to discover rubies in Nam Nga Stream at Mong Hsu (Hlaing 1994), and many miners have traveled from Mogok to work at the new locality. In and along the waterways, the gravels are removed and washed in simple baskets. Ruby-bearing gravel layers (known as *byon*) in the surrounding area are reached by: (1) digging holes from the surface into which the miner is lowered (and the gravels removed) by a simple rope and pulley system; (2) excavating horizontal tunnels into the hill itself, at the level of the gravel layer; and (3) open-pit mining, with the gravels sorted and recovered by sometimes elaborate sluicing systems (figure 5). At some mining sites, mechanized sieves are used to work the gravels (Hlaing, 1994).

Figure 4. Holes and shafts dug to mine the gem-bearing gravels penetrate the hillsides at Mong Hsu in this 1993 photo by V. Yothavut.

CUT STONES AVAILABLE IN THE MARKET

The vast majority of faceted Mong Hsu rubies found on the world market are heat treated, and there is a wide range of qualities. Large quantities of transparent stones with fine red color were available in 1993 and 1994 in sizes up to 0.7 ct (see, e.g., figure 6). Stones of good to very good color and clarity were found in the 1–2 ct range. Stones between 3 and 5 ct were found to be mostly of medium to good quality. These observations are consistent with those reported recently in the trade press ("Rains wash out Mong Hsu supply," 1994). Clarity may be reduced in samples of all sizes by translucent zones of dense white clouds or by the presence

Figure 5. At the Mong Hsu ruby occurrence, an elaborate sluicing system brings the gravels down this hillside for processing. Photo by V. Yothavut.

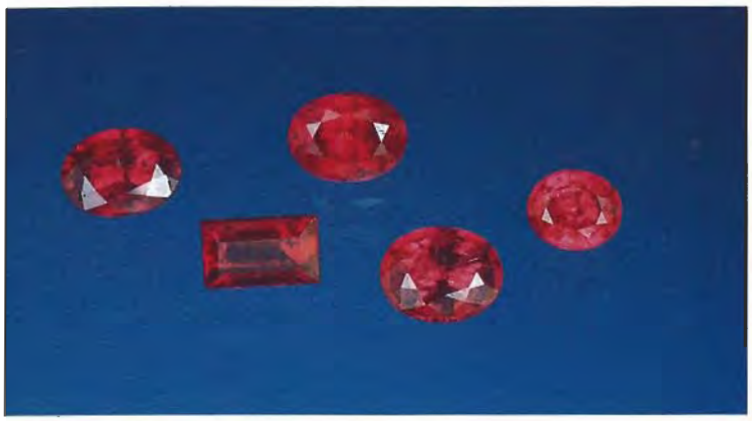

Figure 6. Mong Hsu rubies are typically heat treated, to produce a well-saturated red hue as shown here. Like most of the faceted stones produced to date, these Mong Hsu rubies, from the study sample, are small, 0.348 to 0.683 ct. Photo by Shane F. McClure.

of fingerprint-like inclusions and cracks (see "Microscopic Features" below).

In many of the faceted rubies examined for this study, foreign fillings—such as glass-like substances—were found in fissures and surface cavities (again, see "Microscopic Features" below). Gem laboratories in Asia have reported seeing glass fillings in more than 50% (and, one Thai laboratory, in as much as 90%) of the Mong Hsu rubies examined to date ("Glass filled rubies increasing," 1994). Stones above 5 ct with excellent color and clarity, and no evidence of foreign fillings, appear to be extremely rare.

Fillings in large fissures and cracks improve the apparent clarity of the stones considerably (Peretti, 1993; Milisenda and Henn, 1994). They result from heat treatment in borax or a similar substance, but heat treatment in chemicals is not necessary to alter the violet cores of color-zoned stones to red, as shown by heat-treatment experiments performed in Germany (see figures 7 and 8). According to information obtained in Bangkok, some commercial Thai laboratories use a two-step procedure to heat treat Mong Hsu rubies. First, the samples are heated, without the use of borax, to remove the violet color. Then, the rubies are heated in a borax container to fill fissures and thus enhance apparent clarity. Consequently, some Mong Hsu rubies that have fractures filled with a foreign substance have been treated for both clarity and color enhancement. In these cases, glass or other foreign fracture fillings are not simply an "inadvertent" by-product of heat treatment conducted to remove the blue color component in the samples, as some in the trade have claimed.

Because rubies with artificially filled fractures must be sold as treated, large lots of Mong Hsu rubies containing many stones with such fillings were rejected by European dealers and returned to Bangkok in 1993. In addition, some fracture-filled Mong Hsu rubies have been misidentified as flux-grown synthetic rubies. Some Thai companies have tried to remove the fillings through acid treatment or by recutting the stones. These problems—and others, such as the high volume of production—caused a steep drop in the price of Mong Hsu rough

Figure 7. Heat treatment (in Germany) produced the dramatic color change (right) in this Mong Hsu crystal, which was originally almost black (left). Total length, about 6 mm.

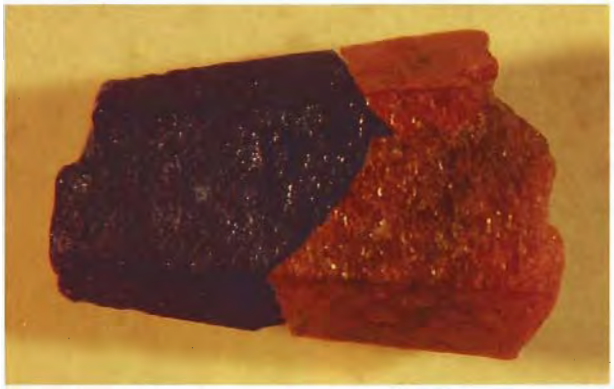

Figure 8. This 8-mm-long Mong Hsu crystal has been cut to show the effect of heat treatment on the core area. The right half is the original (untreated) control sample; with heat treatment, the left half is now a solid red.

at Mae Sai and Bangkok in 1993, to nearly half of its peak (see, e.g., Koivula et al., 1993b; Kammerling et al., 1994; Hlaing, 1994).

CHARACTERISTICS OF MONG HSU RUBIES

Materials and Methods. In addition to the six rough samples provided by MGE in September 1992 and the 74 faceted stones obtained in October 1992 from a Munich dealer, we subsequently saw and examined several parcels of untreated and heat-treated rough and faceted Mong Hsu rubies in both the Bangkok and European markets. Using as our guide the unusual gemological properties (e.g., growth features) of Mong Hsu rubies that we had determined by late 1992, we were able to select parcels of stones that we were confident were free of rubies from other localities for further examination. As of summer 1993, we had selected approximately 50 rough samples and 100 faceted stones—most less than 1 ct (again, see figure 6), with a few up to 2.5 ct—for this research project. In addition, during separate visits to northern Thailand in mid-1993, two of the authors (AP and FM) saw large quantities of untreated Mong Hsu rubies that had entered Thailand at Mae Sai. We purchased several parcels of selected samples for this study. After preliminary examination of about 1,000 carats (in sizes up to 5 ct) of the material obtained at Mae Sai, which was top-quality rough, we selected a parcel of 23 rough, untreated pieces for further study (see, e.g., figure 9). In addition, we examined a great number of the samples selected at Mae Sai after they had been heat treated in Chantaburi, Thailand; from these, we selected nine for further study in Europe. One of the authors (KS) also heat treated about 15 Mong Hsu samples in Germany.

In summary, we had access to more than 200 cut and about 100 rough gem-quality rubies, which we were confident were of Mong Hsu origin, for detailed gemological and mineralogic studies.

We performed standard gemological testing on about 50 of these samples (faceted stones and rough with polished windows). To characterize the internal and external growth planes, we studied approximately 200 samples total (about 60% of which were faceted) using a Schneider horizontal (immersion) microscope with a specially designed sample holder and with specially designed (to measure angles) eyepieces (Schmetzer, 1986a; Kiefert and Schmetzer, 1991; see box A); an additional 12 rough crystals were examined with a standard goniometer. We studied and photographed the inclusions using the Schneider microscope with Zeiss optics as well as an Eickhorst vertical microscope with Nikon optics (the latter with fiber-optic illumination).

Figure 9. We selected these untreated pieces of Mong Hsu ruby rough from our study sample to illustrate some of the many different forms in which this material occurs. The first two rows are typical barrel-shaped, well-terminated crystals; the third row shows flat samples that are sometimes seen, which possibly formed in narrow veins; the waterworn crystals in the fourth row represent a minor proportion of the ruby lots. For an idea of size, note that the crystal on the far left in the upper row is approximately 8 mm long.

Solid inclusions were identified by Raman microprobe spectroscopy, using an X-Y Dilor instrument, as well as by a Philips scanning electron microscope with a Tracor energy-dispersive X-ray spectrometer (SEM-EDS).

Bulk chemical analyses of five untreated rough and five heat-treated cut stones of variable color saturation were performed by energy-dispersive X-ray fluorescence (EDXRF) using a Tracor Northern TN 5000 system. The analyses yield the mean chemical

BOX A: Determination of Growth Structures

The determination of a gem's structural properties, such as straight growth planes that parallel the external faces of the original crystal, or twin planes, is becoming increasingly important as an additional, easily performed method to characterize natural and synthetic gemstones. It requires a microscope, an immersion cell, and immersion liquids (see, e.g., Kiefert and Schmetzer, 1991, for a detailed discussion of the apparatus used for this report). Also useful for the determinative procedures in a horizontal microscope are (1) a biaxial or triaxial sample holder with a dial attached to its vertical axis, and (2) a rotary measuring eyepiece with cross hairs attached to the lens and a dial attached to the ocular tube.

The basic habit of corundum consists of a small number of significant crystal forms: the basal pinacoid, the hexagonal prism, the positive rhombohedron, and the negative rhombohedron, as well as different hexagonal dipyramids. The angles formed by one crystal face and the c-axis, as well as those formed by two distinct crystal faces, are fixed and well known. The biaxial sample holder is used to determine crystal faces by measuring the angle between the optic axis of the ruby crystal and families of straight, parallel growth planes. The measuring eyepiece is used to determine the angles between two different families of straight, parallel growth planes independent of the orientation of the crystal's optic axis.

The first step in examining a faceted ruby is to locate the stone's optic axis and orient it so that it is parallel to the axis of the horizontal microscope. With the stone in this orientation, which is easily accomplished by interference figures seen with crossed polarizers, the gemologist can determine the growth planes by tilting the gem in the direction the optic axis is inclined *vis á vis* the microscope axis. The angle between the optic axis and a family of straight parallel growth planes can be read on the sample-holder dial.

For Mong Hsu rubies, traces of the hexagonal dipyramid ω are sharply outlined with the optic axis inclined about 5° from the microscope axis (as illustrated in figure A-1, right). When Mong Hsu rubies are examined in a direction about 30° inclined to the c-axis, traces of growth planes parallel to the positive rhombohedron *r* and the hexagonal dipyramid *n* can be seen (figure A-1, left).

As a second step, the gemstone should be rotated through 90° toward an orientation in which the optic axis is parallel to the vertical axis of the sample holder. In this orientation, the growth structures parallel to the basal pinacoid *c* are easily recognized. As the gem is rotated about the vertical axis of the sample holder, growth structures parallel to rhombohedral faces and to different hexagonal dipyramids can also be seen. After each rotation through 30°, another series of growth planes becomes visible, and identical planes are repeated after each rotation through 60°.

For Mong Hsu rubies, this second step reveals characteristic growth planes that typically consist of *c*, ω, and *n* (figure A-2, left). After rotation through 30°, a characteristic pattern formed by *r* and *c* usually becomes visible (figure A-2, right).

composition of a surface exposed to the X-ray beam (approximately 2 mm in diameter). Sixteen elements (Al, Mg, Si, P, K, Ca, Ti, V, Cr, Mn, Fe, Ni, Cu, Ga, Zr, Nb) were analyzed with software provided by the manufacturer, which normalizes the resulting oxide percentages to 100 wt.% totals.

Five faceted and three rough samples were analyzed by electron microprobe (CAMECA Camebax SX 50), using an acceleration voltage of 20 kV; standard materials of corundum (Al_2O_3), rutile (TiO_2), eskolaite (Cr_2O_3), hematite (Fe_2O_3), and Mn and V metals; and counting times of 60 seconds for each element (necessary to detect traces of, e.g., iron). To evaluate the inhomogeneous chemical compositions of the samples, between two and seven traverses of 30 to 50 point analyses each were measured across the cores and outer areas of the five faceted and two of the rough samples. A more detailed examination, with four scans of 600 to 800 point analyses each, was performed on the third rough sample (figure B-1), which was extraordinary. We had the samples oriented so that the visible color zoning between the core and the rim could be traversed.

Spectral data of 25 representative samples, including untreated rough and heat-treated cut stones, were obtained with a Leitz-Unicam SP 800 UV-VIS spectrophotometer. Infrared spectroscopy was carried out on 15 heat-treated samples using a Pye-Unicam 9600 FTIR spectrometer and a diffuse-reflection unit.

Crystallography. Facet-quality Mong Hsu rubies are typically well-terminated, barrel-shaped crystals

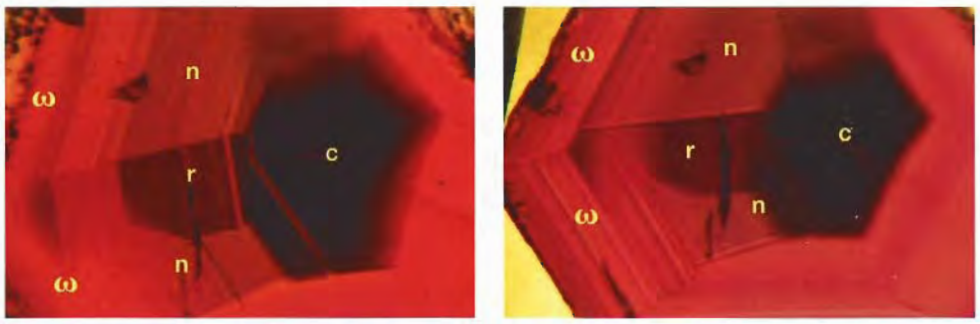

Figure A-1. Mong Hsu ruby slice (about 4.5 mm wide), cut perpendicular to the c-axis: inclined about 5° to the c-axis (right), ω planes are sharp; inclined about 30° (left), r and n planes are sharp. Immersion.

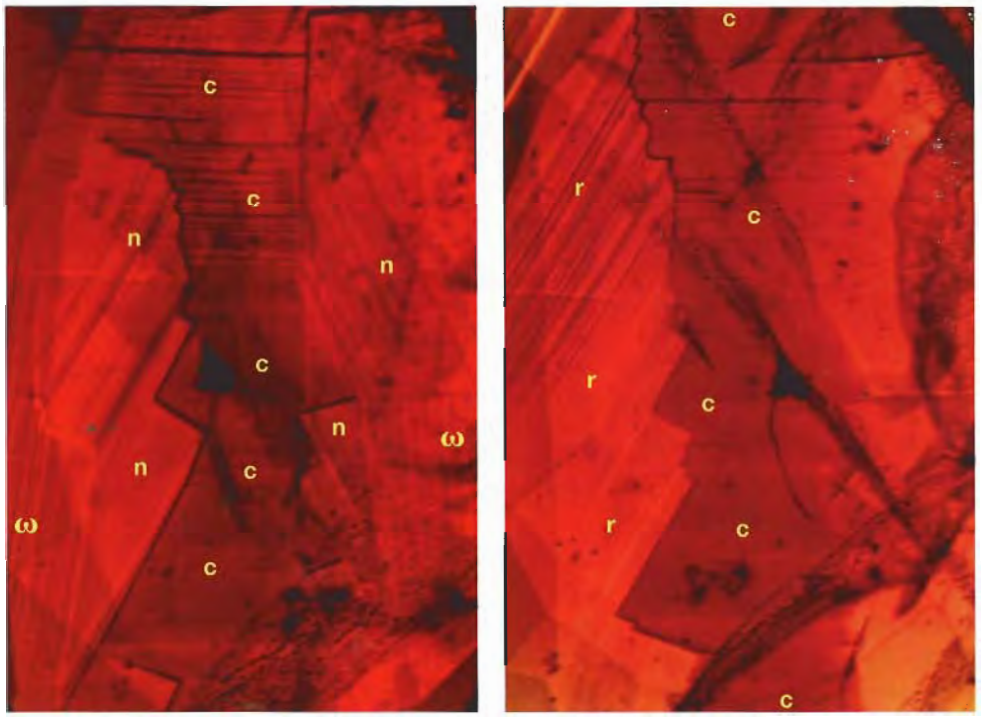

Figure A-2. In this heat-treated and faceted Mong Hsu ruby, the intense red "core" is confined to growth faces parallel to the basal pinacoid c; lighter red areas are confined to two hexagonal dipyramids n and ω (left) and to the positive rhombohedron r (right). View perpendicular to the c-axis; during a rotation of the stones through 30° about the c-axis, two different sharp outlines of growth structures are visible. Immersion, magnified 50×.

(figure 10). Two major habits were observed (figure 11): The first is dominated by the hexagonal dipyramid ω (14 14 $\overline{28}$ 3) and by the basal pinacoid *c* (0001), with a subordinate positive rhombohedron *r* (10$\bar{1}$1). The other habit shows additional hexagonal dipyramids *n* (22$\bar{4}$3). Only minor amounts of water-worn crystals were found in the lots examined.

Another form of Mong Hsu ruby is extremely flat, possibly due to growth in narrow veins (again see figure 9). Crystals with this morphology, in general, are not useful for jewelry purposes and were therefore not included in this report.

Visual Appearance. Less than 5% of the rough Mong Hsu samples we examined were a uniform red or violet to almost black. Most stones from this locality show a distinct color zoning, with transparent red outer zones ("rims") and violet to almost black centers (commonly called "cores") that appear opaque to translucent (again, see figures 9 and 10). In thin section, a core that originally looked almost black and opaque will undoubtedly appear violet and transparent (see, e.g., figure 2). Depending on what part of the original crystal a fragment represents, great variability in color and color zoning is observed in lots of the rough. A more detailed description of this extraordinary color zoning is presented in "Microscopic Features" below.

Heat treatment removes the violet component of the cores to produce stones that are uniformly red, as confirmed by experiments carried out in Germany (see figures 7 and 8). There is, however, some variation in the shades of red seen in the heat-treated samples. In addition, in some of the rough

Figure 10. A well-formed Mong Hsu crystal consists of two hexagonal dipyramids, ω and n, *the positive rhombohedron* r, *and the basal pinacoid* c, *as illustrated by this 5-mm sample. Note the violet core.*

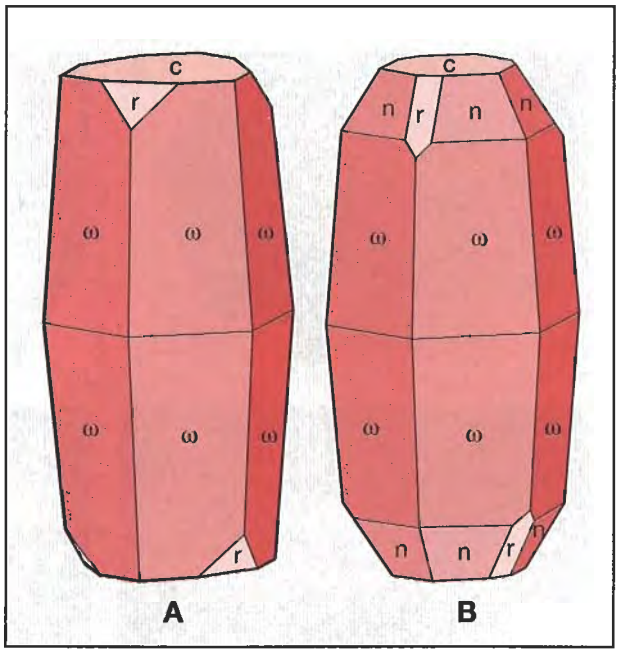

Figure 11. The crystal habit of Mong Hsu rubies consists of two hexagonal dipyramids, n *(22$\bar{4}$3) and* ω *(14 14 $\overline{28}$ 3), the basal pinacoid* c *(0001), and the positive rhombohedron* r *(10$\bar{1}$1). The crystal drawn on the left is dominated by* ω *and* c *faces, with a subordinate* r *plane; the crystal shown on the right is dominated by* ω *and* c *faces, with subordinate* r *and* n *planes.*

heat treated commercially, we observed translucent, highly reflecting, whitish zones that made the stones unsuitable for faceting. As a result of these whitish zones, a percentage of the material is rejected after heat treatment. Although distinct color zoning is usually not visible with the unaided eye, microscopic examination reveals a highly characteristic type of color zoning related to specific growth structures in most of the heat-treated samples—with intense red related to core zones and lighter red related to rims.

Gemological Properties. The distinctive color distribution in Mong Hsu rubies is also reflected in some of their gemological properties (table 1).

UV Fluorescence. The differences between cores and rim areas are well illustrated by their reactions to long- and short-wave ultraviolet radiation. In untreated samples, the cores are inert or fluoresce light orange to light red, whereas the rims fluoresce intense orange-red to red. This difference is less obvious after heat treatment: The cores of heat-treated samples fluoresce orange-red to red, whereas the rims remain intense orange-red to intense red.

Optical Properties. We found the variations in refractive index among the different samples to be unusually high for both the ordinary and extraordinary rays, with a slightly variable birefringence between 0.008 and 0.010 (see table 1). A similar large variation in R.I.'s was reported by Smith and Surdez (1994) for rubies from Mong Hsu, and was recently described for rubies from Malawi that revealed highly variable amounts of trace elements, especially chromium (Bank et al., 1988).

We also found differences in R.I. between cores and rims of both heat-treated and untreated Mong Hsu samples. For example, one rough sample that was sawn and polished revealed R.I.'s of n_o = 1.774 for the core and 1.770 for the rim, n_e = 1.765 for the core and 1.762 for the rim (birefringence = 0.009 and 0.008, respectively).

Therefore, depending on the orientation of the table facet with respect to the optical axis and the portion of the original crystal the table encompasses, different refractive indices are possible. If the table facet is largely confined to one single growth zone (see "Microscopic Features" below and boxes A and B), sharp shadow edges are observed for the ordinary and the extraordinary rays on the refrac-

TABLE 1. Gemological characteristics of Mong Hsu rubies.[a]

Property	Untreated samples		Heat-treated samples	
	Core	Rim	Core	Rim
Color	Violet to black	Red	Intense red	Red
Pleochroic colors				
Parallel to *c*	Light bluish violet to reddish violet	Orange-red	Orange-red	Orange-red
Perpendicular to *c*	Intense bluish violet to reddish violet	Purplish red	Purplish red	Purplish red
Fluorescence				
Long-wave UV	Inert or light orange	Intense orange red	Orange red	Intense orange-red
Short-wave UV	Inert or light red	Intense red	Red	Intense red
Specific gravity (range)	3.990 - 4.010			
Refractive indices (range)				
n_o	1.768 - 1.780			
n_e	1.760 - 1.770			
Birefringence	0.008 - 0.010			

[a] *For the ordinary type of samples with violet to black cores and red rims.*

tometer (table 1). This is often the case for samples with table facets cut parallel to the c-axis or for samples with small cores. If the table facet encompasses a "mixed" area—that is, part is from the core and part is from the rim, the shadow edges are often less distinct and in extreme cases no readings are visible on the refractometer. Typically, this is the case with a stone on which the table facet is oriented perpendicular to the c-axis, with an intense red central core and a lighter red rim. All intermediate situations are observed for faceted samples with random orientation.

This unusual variation in refractive indices within one crystal is usually caused by the chemical zoning between cores and rims, but it also may occur between different zones within cores and outer areas (see "Chemical Properties" and box B).

Other gemological properties of the Mong Hsu rubies tested, such as pleochroism and specific gravity (table 1), were consistent with those of natural rubies from other localities. Note that the color of the untreated cores appeared intense violet perpendicular to the c-axis and somewhat lighter violet parallel to the c-axis.

Microscopic Features. *Growth Structures and Color Zoning in Untreated Mong Hsu Rubies.* By determining the internal growth structures in a cut stone, the gemologist can reconstruct the habit of the original ruby crystal. (Again, see box A for the procedures used in this study.) Changes in the habit during growth and color zoning characteristics also can be studied (see, e.g., box B.)

Well-preserved Mong Hsu corundum crystals are defined by *c*, *r*, *n*, and ω faces. These growth features can also be observed in faceted stones or in fragments of rough stones as thin traces of growth planes parallel to the former external faces of the ruby.

Because of the complex growth sequence established for Mong Hsu rubies (see box B), crystals and crystal fragments also reveal distinctive color zoning. Samples that are homogeneous in color (suggesting crystal growth in a single phase) occur only rarely. These are, for example, red with c, *r*, *n*, and ω faces (again, see figure 9) or dark violet to almost black with *c*, *r*, and ω faces (again, see figure 7). The most common pattern in Mong Hsu rubies, however, consists of a dark, nontransparent core and a red outer zone (see again Figure 2).

An even more complex pattern is formed in samples that contain two dark violet "cores" that are separated by a red layer along the c-axis (figure 12). In a view parallel to the c-axis, a dark core in the center is followed by a light red zone, a second lighter violet zone (representing the second "core"), and an outer red rim. In a very few instances, we observed Mong Hsu rubies with a thin, intense red rim confined to *n* or ω faces (figure 13). The thin red rims represent the latest stage of growth for these samples in which an enrichment of chromium took place.

A modification of the typical habit and color zoning in Mong Hsu rubies is shown in figure 14. The violet-to-black color in this extraordinary ruby forms only in growth zones parallel to basal planes,

BOX B: Color Zoning and Habit Changes in Untreated Mong Hsu Rubies

The most distinctive, characteristic feature of untreated Mong Hsu rubies is their color zoning. Although two zones are usually evident—violet "cores" and red "rims"—the zoning in Mong Hsu rubies is actually somewhat more complicated than this.

Most Mong Hsu ruby crystals consist of one (or, rarely, two) violet to almost black cores with intense red rims. An extraordinary sample with two dark violet "cores" separated by an intense red zone (figure B-1) best reveals this general scheme for color zoning related to growth history. The duplicate sequence identified in this stone (table B-1) confirms the "single" characteristic sequence observed in most Mong Hsu rubies (an exception is the stone illustrated in figure 14).

Red growth zones (R) consist of red (ruby) layers parallel to the basal pinacoid *c*, to the positive rhombohedron *r*, and to two hexagonal dipyramids, *n* and *ω*. Because all four faces (*c*, *r*, *n*, and *ω*) have growth rates greater than zero, red layers form parallel to all four.

Violet (V) growth zones consist of violet (sapphire) layers parallel to *c*, *r*, and *n*. In V growth zones, only these three faces reveal growth rates greater than zero; *ω* growth rates are not observed. This indicates that *ω* dominates the external crystal form, although no violet layers grow parallel to *ω*.

Along the c-axis of the ruby shown in figure B-1, which is schematically drawn in figure B-2, the V zones in the center of the crystal abruptly convert to R zones. The R zones then gradually convert to intermediate (I) zones, which subsequently convert to violet (V') zones. The I zones consist of alternating thin red layers parallel to *c*, *r*, *n*, and *ω*, and small violet layers parallel to *c*, *r*, and *n* (again, see table B-1; also see figure B-3), but not *ω*.

In summary, along the c-axis of the crystal described, the following cyclic sequence of growth zones is observed:

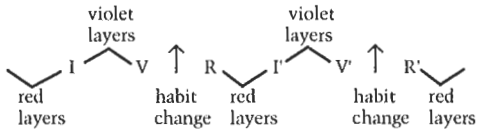

Each of the two violet "cores" in this crystal consists of violet layers parallel to *c*, *r*, and *n* faces, which form in subsequent I and V growth zones. Over the two violet cores are red layers parallel to *c*, *r*, *n*, and *ω*, which grow in subsequent R and I zones. Those parts of the "cores" that formed during V are usually dark violet and translucent to almost opaque black; those that formed during I are lighter violet and translucent to transparent.

We have found the growth sequence R I V to apply to most of the Mong Hsu rubies examined. Note that in some crystals, stage R is very small. Others

Figure B-1. This 10.5-mm-long untreated crystal, with two violet cores surrounded by red areas, illustrates the relationship between growth conditions and habit change typical of Mong Hsu rubies.

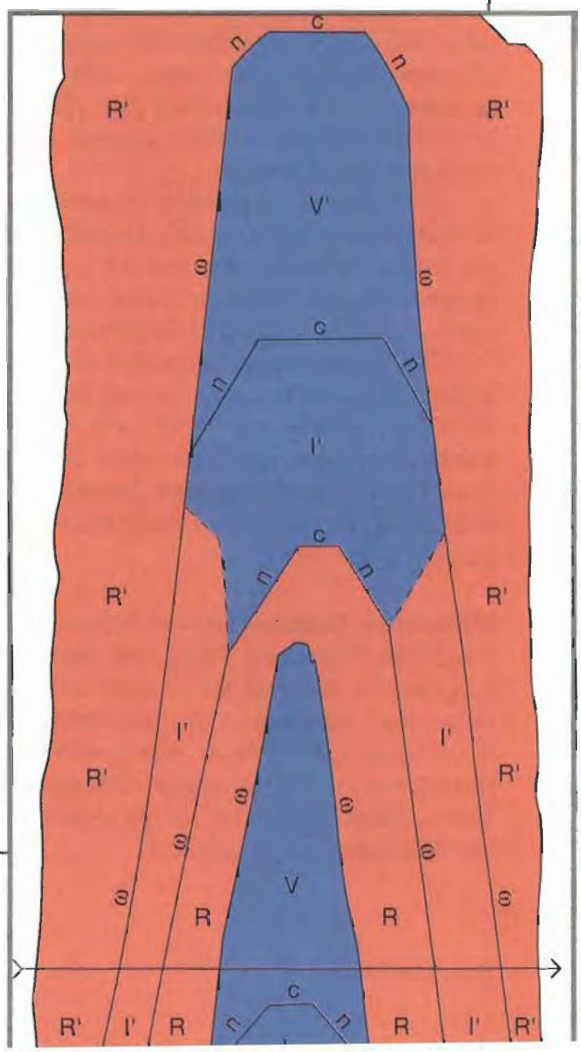

Figure B-2. This schematic representation of habit change and color zoning in the center of the Mong Hsu ruby in figure B-1 shows the R (red), V (violet) and I (intermediate) growth phases seen in the following growth sequence (from bottom): I V R I' V' R'. The arrow indicates the position of a microprobe scan.

were grown during a period that did not cover the full R I V growth sequence; such a crystal may consist only of a dark violet, nontransparent core grown in stage V, and a red rim grown in stage R.

Also notable in Mong Hsu rubies with the R I V growth sequence is the decreasing size of the hexagonal dipyramid *n*. During growth phase R, relatively large *n* faces form (see, e.g., figure 11B). In the subsequent zones I and V, *n* is progressively smaller; in the end stage of phase V, *n* is absent (figure 11A). Consequently, with an abrupt change of growth conditions from stage V to stage R, there is also a distinct habit change.

In summary, at the beginning of growth stage R, the crystal habit consists of *c*, *r*, *n*, and *ω* faces (figures 10 and 11B). In the growth sequence R I V, the growth rate of *n* strongly increases until, at the end of stage V, it disappears completely. Concurrently, the growth rate of face *ω* reaches zero, so *ω* dominates the external crystal form (figures 11A and 7). To date, we have seen no systematic change in the *r* and *c* faces over the sequence R I V in the samples available.

The complex growth structure of Mong Hsu rubies is reflected by a complex chemical zoning. For the sample pictured in figure B-1, four microprobe traverses, with 600 to 800 point analyses each, were performed. The position of one of these scans across the sample (including 700 equidistant analysis points) is shown in figure B-2. It twice crossed three red *ω* growth zones R', I', and R, as well as violet *n* and *c* growth layers belonging to the V area. The profile revealed that chromium values are symmetrical in both areas right and left of the center of the crystal; in general, chromium contents are higher in the violet core of growth zone V than in the R', I', and R growth zones. Again, in the violet core, differences between areas related to the basal pinacoid *c* (1.20–1.35 wt.% Cr_2O_3) and areas related to dipyramidal *n* growth faces (0.90–0.95 wt.% Cr_2O_3) were also measured. Chromium contents in the red R and I' zones of the rim (0.63–0.75 wt.%) are generally lower than in the violet core.

In the small area between two adjacent *ω* growth zones in the red rim (i.e., between I' and R'), the scan reveals a distinct decrease from about 0.63 to 0.38 wt.% Cr_2O_3, correlated to an increase from 0.05 to about 0.40 wt.% TiO_2. This represents a growth zone that was present during the formation of the second violet core V'. In the outer *ω* growth zone of R', we recorded a continuous increase (from 0.63 to 0.97 wt.%) in Cr_2O_3, which reaches values in the outermost layers that are similar to the concentration in the core area that is related to *n* faces (see also figure 13).

Average vanadium and titanium contents in the violet core are about twice those measured in the red rim. No distinct zoning of iron was observed in this traverse. The other three scans show even more complex results, but these details are beyond the scope of this article. In summary, the complex color zoning seen with the microscope is reflected by a complex chemical zoning in the sample.

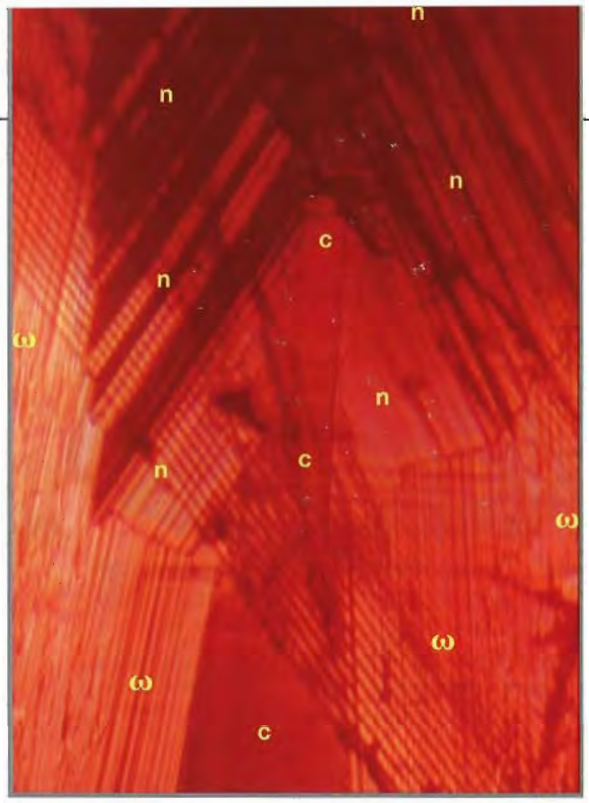

Figure B-3. An enlarged portion of the Mong Hsu ruby in figures B-1 and B-2 shows part of the I' growth zone, with alternating violet and red layers parallel to n, *and red layers parallel to* ω. *Immersion, magnified 50×.*

TABLE B-1. General outline of habit change in different growth phases (R, I, V) of Mong Hsu rubies.[a]

Variables	R (red)				I (intermediate)				V (violet)			
	c	*r*	*n*	*ω*	*c*	*r*	*n*	*ω*	*c*	*r*	*n*	*ω*
Growth rate	Mod.	Mod.	Slow	Slow	Mod.	Mod.	Mod.	Alternating slow/none	Mod.	Mod.	Very fast	None
Layers formed	Yes	Yes	Yes	Yes	Yes	Yes	Yes	Alternating yes/no	Yes	Yes	Yes	No
Relative sizes of faces	Mod.	Mod.	Large	Very large	Mod.	Mod.	Mod.	Very large	Mod.	Mod.	Very small or absent	Very large
Variety	Ruby				Alternating ruby/violet sapphire				Violet sapphire			
Habit	*c*, *r*, *n*, *ω* (figure 11) *n* is large				*c*, *r*, *n*, *ω* *n* becomes smaller				*c*, *r*, *ω* (figure 11) *n* is very small or absent			

[a]*Habit changes from R to I and from I to V are continuous; the habit change from V to R is abrupt.*

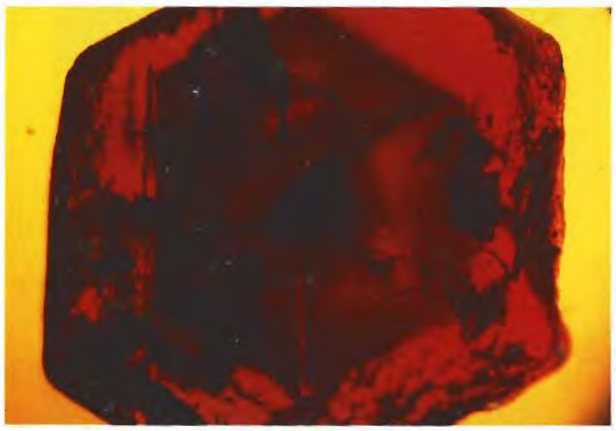

Figure 12. This untreated piece of Mong Hsu rough revealed a complex growth history: A small black core in the center is surrounded by a first red layer, over which is a second violet zone that, in turn, is surrounded by a red layer. View parallel to the c-axis, immersion, magnified 40×.

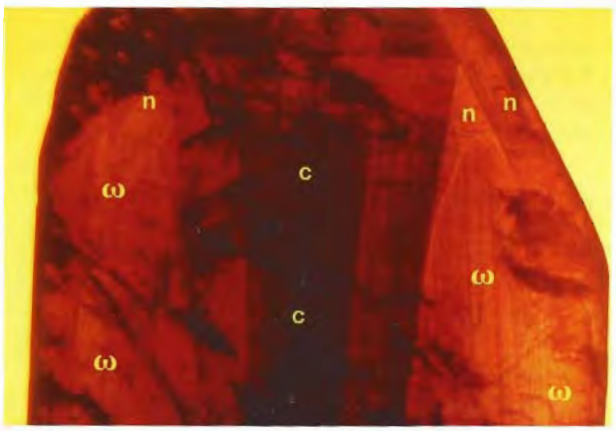

Figure 14. Unlike most of the other Mong Hsu rubies examined for this study, the violet core in this untreated rough sample is confined only to the basal c *face, while* n *and* ω *growth planes are red. The size of the basal plane increases toward the outer zone of the crystal, in a wedge-shaped pattern. View perpendicular to the c-axis, immersion, magnified 30×.*

Figure 13. In this untreated Mong Hsu fragment with n *and* ω *growth planes, an intense red stripe confined to a natural* n *face represents the latest growth stage. View perpendicular to the c-axis, immersion, magnified 30×.*

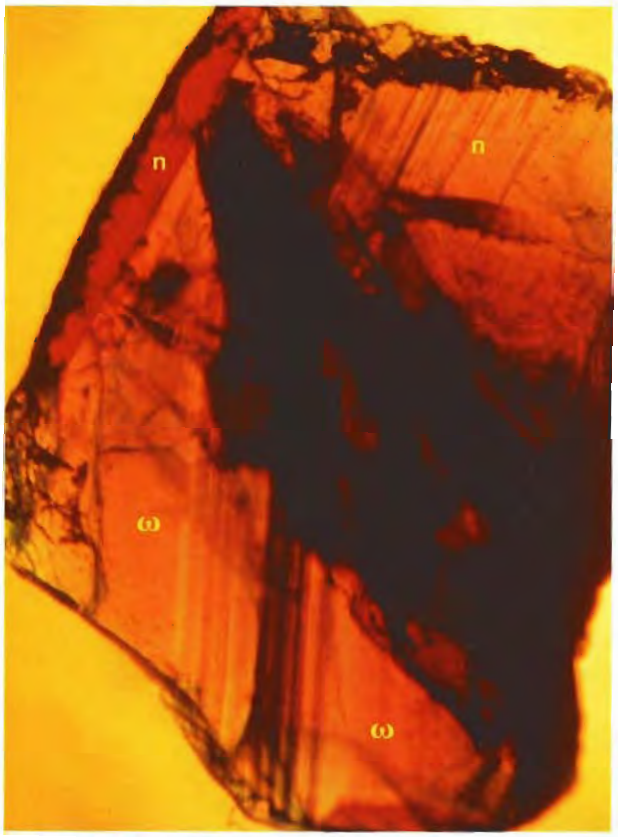

whereas growth planes parallel to *n* and *ω* are red. We also observed that the *c*-plane increased in size during growth, in a direction toward the outer faces of the crystal. Thus, the violet portion in the stone appeared as a wedge-shaped pattern in the rough crystal, with the base of the wedge confined to the latest growth area. In another sample, which also had a wedge-shaped growth pattern confined to the basal plane, dark violet areas were developed as small stripes parallel to *ω*, and lighter violet stripes were observed parallel to *n*, but areas confined to *c* and *r* growth zones were red.

Growth Structures in Heat-Treated Rubies. Some of the growth characteristics related to natural color zoning are not observed in cut Mong Hsu rubies, because part of the growth history of a crystal is lost during cutting and heat treatment turns the violet cores red. However, neither cutting nor heat treatment alters the characteristic internal growth planes, which we were able to identify in most of the faceted Mong Hsu rubies examined.

Due to the fact that these same patterns and combinations of patterns have never, to the best of our knowledge, been observed in natural rubies before, we feel they are useful to distinguish Mong Hsu rubies from rubies from other localities. In other words: The individual crystal faces observed in Mong Hsu rubies have been identified in rubies from other sources, but the overall pattern of color zoning and habit—that is, the combination of faces

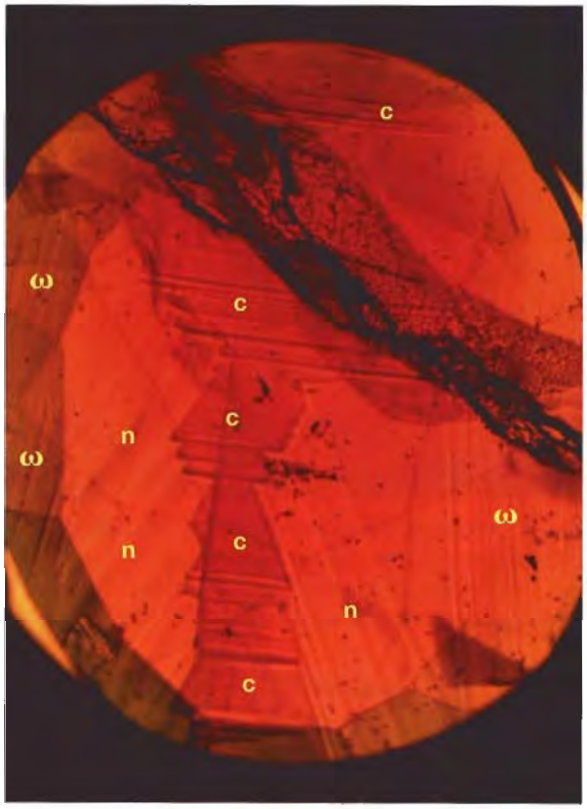

Figure 15. This faceted, heat-treated Mong Hsu ruby is typical of most of the cut Mong Hsu rubies we examined. An intense red core is confined to faces parallel to the basal c *plane, the size of the basal plane varies irregularly along the c-axis, and the lighter red areas are confined to* n *and* ω *growth zones. View perpendicular to the c-axis, immersion, crossed polarizers, magnified 40×.*

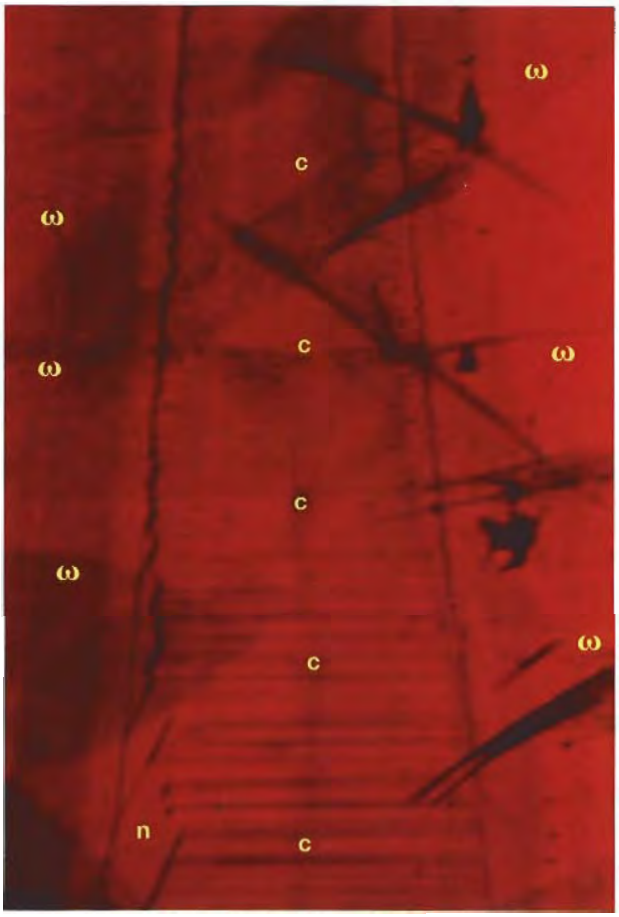

Figure 16. In this faceted, heat-treated Mong Hsu ruby, with dominant growth parallel to c *in the core and* ω *planes in the rim (as is typical for rubies from this locality), only subordinate and small* n *faces are observed in the core. View perpendicular to the c-axis, immersion, magnified 50×.*

and the color zoning related to certain growth zones—has not. In addition, because of their distinctive growth patterns, Mong Hsu rubies can be easily separated from their synthetic counterparts.

Typical examples of growth structures that can be found in heat-treated Mong Hsu rubies are shown in figures A-2, 15, and 16. In most of our samples, dark red color zones were confined to basal *c* growth planes of variable size (figure 15). These dark red zones are surrounded by lighter red areas with growth planes parallel to *r*, *n*, and *ω* (figure A-2). Because faceted stones represent only one area within the original crystal, in the complex growth sequence of Mong Hsu rubies (see box B) the growth zones confined to *n* faces may be extremely small or absent (figure 16).

Twinning. Twinning is encountered only infrequently in Mong Hsu rubies. The most common type appears to be a repeated rhombohedral twinning, predominantly in one direction parallel to one rhombohedral *r* face. We observed particles confined to intersection lines of twin planes in only two of our samples, which confirms that rubies with two directions of rhombohedral twinning parallel to two *r* faces are extremely rare from this locality.

Solid Inclusions. Only rarely did we observe solid inclusions other than whitish particles (see below) in the Mong Hsu rubies examined. These include rutile and fluorite (figure 17; both identified by Raman spectroscopy and SEM-EDS), as well as spinel, which was identified by Raman spectroscopy. Dolomite was identified by SEM-EDS analysis in one crystal; it occurred as a series of rounded, transparent inclusions throughout the red portion. Dolomite was also identified by Smith and

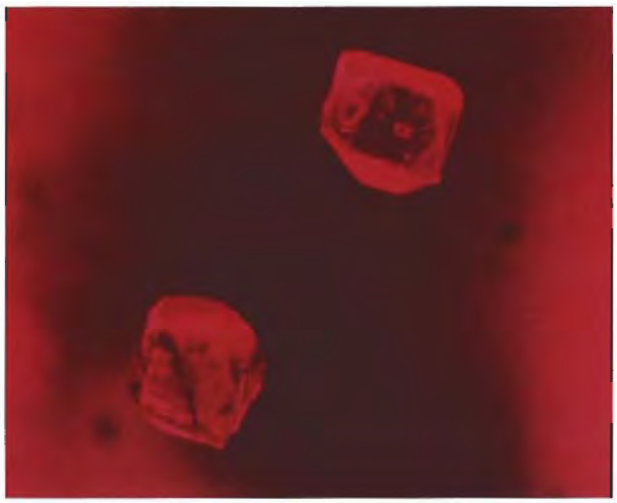

Figure 17. Fluorite (left) and spinel (right) are among the few solid inclusions observed in Mong Hsu rubies. Fiber-optic illumination, transmitted and reflected light; diameter of the solid inclusions is approximately 0.2 mm.

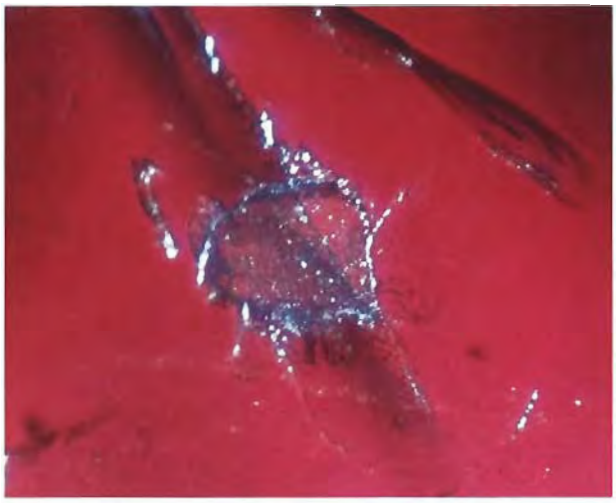

Figure 18. White Mg-chlorite was identified in the outermost parts of some untreated Mong Hsu rubies. Fiber-optic illumination, reflected and transmitted light, magnified 90×.

Surdez (1994) in Mong Hsu rubies; they found apatite as well.

As noted earlier, white mica, fuchsite, and Mg-chlorite were found as overgrowths on some rough Mong Hsu specimens. Mg-chlorite and white mica also were identified by Raman spectroscopy (based on the reference work of Prieto et al., 1991) as inclusions in the outermost parts of some rough crystals (figure 18). It appears that they are, in most cases, removed during preforming of the rough before heat treatment.

Whitish Particles. Various types of small particles ("whitish dust") also are found in both the untreated rough and heat-treated cut Mong Hsu rubies. These particles represent one of the most characteristic inclusion features compared to rubies from other natural sources, and so they are useful in separating Mong Hsu rubies from those from other sources or from synthetic rubies (see also Laughter, 1993a and b; Smith and Surdez, 1994). These inclusions are best resolved using fiber-optic illumination. Two types are:

- Whitish streamers that are oriented perpendicular to growth planes (figures 19–21). They usually extend from the outermost edge of the violet core or lie in close proximity to that area. They

Figure 19. This whitish streamer in an untreated Mong Hsu ruby appears to originate from a solid inclusion located at the boundary between the violet core and red rim. Fiber-optic illumination, reflected light, magnified 100×.

Figure 20. A whitish streamer (left) emerges from the end of a pseudosecondary feather of fluid inclusions along the black core of this untreated Mong Hsu. View almost parallel to the c-axis, fiber-optic illumination, transmitted and reflected light, magnified 60×; photomicrograph by E. Gübelin.

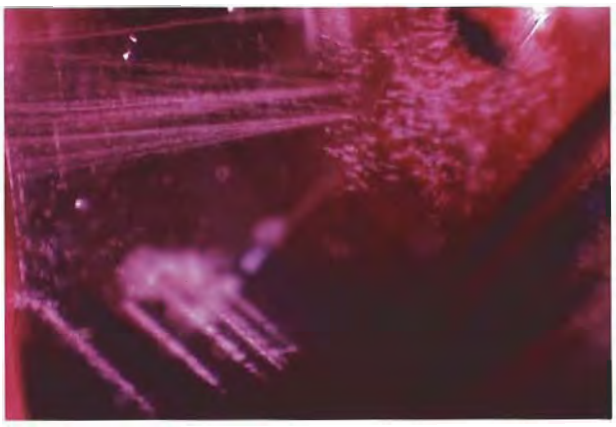

Figure 21. Clouds of snowflake-like particles appear in the upper right of this untreated Mong Hsu ruby, together with a streamer that runs perpendicular to growth structures (top left) and particles confined to ω growth areas (bottom left). View almost parallel to the c-axis, fiber-optic illumination, reflected light, magnified 80×.

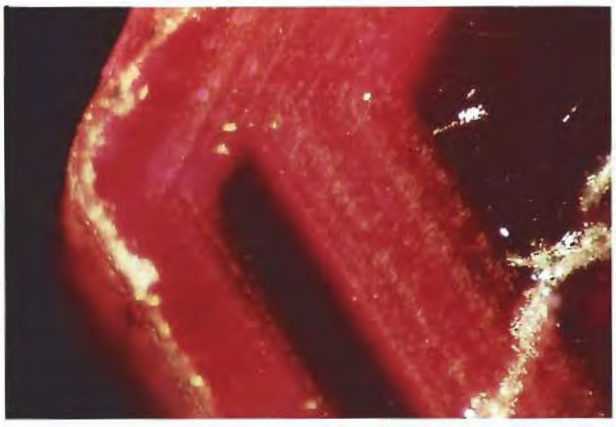

Figure 22. Often the whitish dust-like particles seen in untreated Mong Hsu rubies occurred in zones confined to growth planes. This type of inclusion was not removed by heat treatment. View almost parallel to the c-axis, fiber-optic illumination, reflected light, magnified 60×.

appear to be initiated by the trapping of solid (figure 19) or fluid (figure 20) inclusions, which tend to be concentrated in the boundary zone between core and rim. These initial crystal defects do not completely heal during subsequent growth, and new defects—which also act as traps for fluids—are continuously formed. Ultimately, they appear as a series of lines consisting of small reflecting particles, which are oriented perpendicular to the growth planes of that particular zone.

- Whitish dust, resembling clouds of snowflakes (figure 21), frequently can be seen irregularly dispersed in large zones of a crystal. This type of inclusion is often confined to certain growth zones (figure 22), usually related to the ω plane (figure 21).

Whitish particles of a completely different type are formed by heat treatment. These particles form dense areas, in some cases in ω zones that grew after the originally violet core (figure 23), and occasionally in growth zones confined to the basal face. Note that dense zones of whitish particles were also observed in areas confined to the violet or almost black core. In extreme cases, the whitish particles are so dense that the stone appears semitranslucent, with large whitish reflecting areas, which makes it unsuitable for the jewelry market. In one heat-treated sample, we observed dense, oriented, needle-like particles. We also observed the formation of such needles in another sample heat treated in Germany; they appeared in an area, confined to the rim of the stone, that had originally been transparent red, as well as in violet zones. We do not yet know the exact nature of these needles.

Fluid Inclusions. In contrast to solid inclusions, fluid inclusions were frequently seen in both untreated and heat-treated Mong Hsu rubies, in cores as well as rims. For the most part, they represent various primary fluids trapped in single cavities as well as in pseudosecondary (figure 20) and secondary "feathers" or "fingerprints." They are

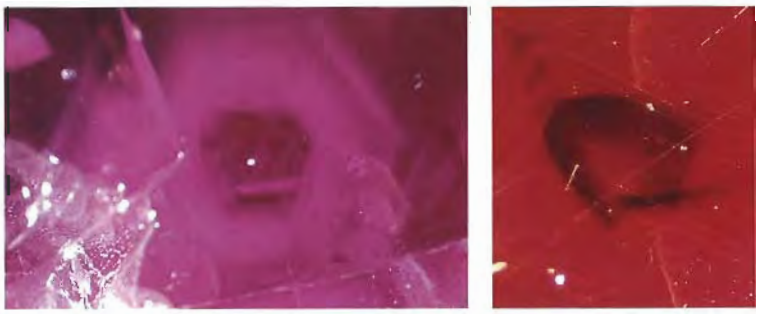

Figure 23. Violet to almost black zones in the center of this Mong Hsu crystal in its natural state (right) were completely gone after heat treatment (left), but whitish particles had formed in ω growth zones outside the center. View almost parallel to the c-axis, fiber-optic illumination, reflected and transmitted light, magnified 60×.

Figure 24. Healing feathers ("fingerprints")—actually interconnecting tubes and isolated dots of fluid inclusions—were commonly seen in both heat-treated (as here) and untreated Mong Hsu rubies. Immersion, magnified 60×.

related to the cracking of the ruby and subsequent healing by fluids.

If this type of inclusion forms early in crystal growth close to the core, the outline of the core is sometimes seen parallel to the border of the "feather" (figure 20). Another "feather" in a heat-treated Mong Hsu ruby (figure 24) consists of isolated droplets and interconnecting tubes. It formed later than the example illustrated in figure 20.

Fracture Fillings Produced by Heat Treatment. Heat treatment may create additional fractures in the ruby because of the decrepitation of solid matter or fluids trapped in small cavities. This reduces the transparency of the stone. As demonstrated by heat-treatment experiments in Germany, no chemicals are needed to remove the blue color component completely from the Mong Hsu stones. As noted earlier, though, commercial treaters often use various chemicals, such as borax, during a second heating process to fill cracks and fissures exposed at the surface and thus enhance apparent clarity (Hughes, 1988; Peretti, 1993; Henn and Bank, 1993). Borax or similar substances can act as a flux to dissolve alumina and can cause, at least partly, a recrystallization or healing of open fracture planes (Hänni, 1992; Koivula et al., 1993a; Milisenda and Henn, 1994). Mica or chlorite present in these open cavities or fissures will dissolve in the presence of borax and form borosilicates that are then trapped as artificial glassy fillings. The formation of a crystalline phase in fractures of treated Mong Hsu rubies has also been observed, and the compound was identified by means of X-ray powder diffraction as aluminum borate (H. A. Hänni, pers. comm., 1994).

We observed fissures and cavities containing these foreign fillers in many Mong Hsu samples obtained from the trade. In some treated rubies, we saw flow structures in the glassy fillers of heavily included samples, which easily identified them as foreign material (figure 25). In contrast, only careful microscopic examination revealed the presence of foreign substances in other, partly recrystallized fractures (figure 26). The exact composition of various filling materials, however, cannot be identified by microscopic examination. In areas in which the filling material reaches the surface of the ruby, the filled fissure can be recognized by its reduced luster

Figure 25. Flow structures can be seen in this fissure, which has been partially filled with a solid foreign material. During heat treatment for clarity enhancement, the host Mong Hsu ruby was placed in contact with borax or a similar substance. Immersion, magnified 60×.

Figure 26. In some partly recrystallized fractures, it is difficult to locate the foreign substance (possibly borax or an aluminum borate) to which the ruby was exposed during heat treatment. Immersion, magnified 60×.

TABLE 2. X-ray fluorescence analyses and refractive indices of Mong Hsu rubies.[a]

	Untreated rough					Heat-treated faceted				
Oxide/R.I.	A	B	C	D	E	F	G	H	I	J
Oxide										
Al_2O_3	99.300	98.600	98.400	99.200	98.800	99.000	98.400	98.400	98.900	99.500
Cr_2O_3	0.460	0.914	1.216	0.572	0.594	0.654	1.166	1.391	0.718	0.354
FeO	0.006	0.060	0.031	0.003	0.035	0.003	0.017	0.008	0.007	0.005
TiO_2	0.107	0.194	0.168	0.134	0.338	0.145	0.233	0.046	0.210	0.045
V_2O_3	0.038	0.050	0.057	0.045	0.100	0.090	0.023	0.035	0.090	0.014
Ga_2O_3	0.010	0.010	0.014	0.013	0.017	0.009	0.006	0.011	0.010	0.004
Refractive indices										
n_o	—[b]	1.773	1.774	1.771	1.772	1.771	1.775	1.775	—[b]	1.770
n_e	—[b]	1.765	1.765	1.762	1.763	1.763	1.766	1.766	—[b]	1.762

[a] *The columns do not total 100 wt.% due to traces of MnO, K_2O, MgO, CaO, and SiO_2. No traces of CuO, NiO, ZrO_2, P_2O_5, or Nb_2O_5 were detected.*
[b] *No sharp shadow edges observed on the refractometer.*

compared to that of the polished ruby when viewed with reflected light (see, e.g., Kane, 1984; Scarratt and Harding, 1984; Scarratt et al., 1986; Hänni, 1986).

Chemical Properties. The methods applied to determine the rubies' chemical properties provide analytical data that represent different-size areas within the samples. X-ray fluorescence analysis reveals an average composition of that part of the ruby (in an area that can be measured in millimeters) that was exposed to the X-ray beam, such as part of the table of a faceted stone. The electron microprobe analyzes areas with diameters in the micrometer range. Thus, traverses with several point analyses across the polished surface of a ruby indicate the chemical variability of a sample. For certain trace elements, such as gallium, the more sensitive X-ray fluorescence analysis is required to obtain quantitative data.

The reliability of the data obtained for this study by X-ray fluorescence and electron microprobe analyses is supported by the similarity in average trace-element concentrations reported by both methods.

X-ray Fluorescence Analysis. The results of X-ray fluorescence analyses of various rubies (five untreated and five heat treated) are shown in table 2. The untreated rubies were composed of rough fragments of crystals with plane polished faces. As can be seen from table 2, the rubies contain significant trace-element concentrations of Cr_2O_3, FeO, TiO_2, V_2O_3, and Ga_2O_3. Large differences in the trace-element concentrations among the various samples were measured, but we saw no significant differences in trace-element amounts between treated and untreated stones.

For the eight samples analyzed for which refractive indices could be measured on the refractometer (again, see table 2), a reasonable correlation was found between R.I.'s and chromium concentrations, and a good coincidence was obtained in a plot with the sum of trace-element concentrations (calculated as $Cr_2O_3 + Ti_2O_3 + V_2O_3 + Fe_2O_3 + Ga_2O_3$) versus refractive indices (figure 27). Consequently,

Figure 27. Refractive indices were correlated with chemical composition in the eight Mong Hsu rubies analyzed by X-ray fluorescence for which refractive indices could be measured (see table 2). The correlations are expressed here as the sum of trace-element concentrations; red squares = ordinary ray (n_o), black squares = extraordinary ray (n_e). A distinct increase in refractive indices is caused by increasing trace-element contents.

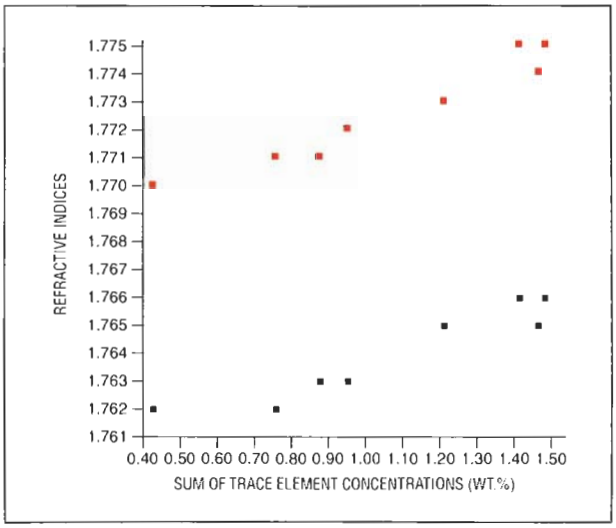

variations in refractive index are related to variations in trace-element contents.

Electron Microprobe Analysis. As the results shown in table 3 indicate, systematic variations within the samples were observed for TiO_2 and Cr_2O_3 and, in some samples, for V_2O_3; only the statistical variations of the analytical instrument were found for FeO and MnO.

On the basis of the relationships between Cr_2O_3 and TiO_2 (in combination with FeO), we have identified three basic types of chemical zoning in Mong Hsu rubies to date (see also box B):

- *Type A*: A distinct variation in Cr_2O_3 that is not correlated to titanium was found for samples 1, 3, and 4 (figure 28A). These rubies had high Cr_2O_3 concentrations in the intense red zone (that represents the core of the original crystal) and lesser quantities of Cr_2O_3 in the lighter red "rim" (samples 1 and 3). In sample 4, we found a less extreme microscopic red color zoning, although the sample was faceted with its table perpendicular to the c-axis. Accordingly, the chemical variations were less pronounced than in other samples with a strong visual color zoning.
- *Type B:* A distinct variation in Cr_2O_3 was found to correlate with a distinct TiO_2 zoning in heat-treated samples 2 and 5 (figure 28B). High concentrations of Cr_2O_3 and TiO_2 were restricted to the relatively intense red core.
- *Type C:* A distinct zoning of TiO_2 perpendicular to the c-axis, inversely correlated to Cr_2O_3 in the outer zones of the rim, was found in untreated sample 6 (figure 28C), which had a homogeneous violet core and a light red rim. TiO_2 concentrations were higher in the core than in the rim. Cr_2O_3 was higher in the outermost part of the rim. No systematic variations

TABLE 3. Electron microprobe analyses of Mong Hsu rubies.

	Faceted sample number[a]					Rough sample number[a]		
Variable	1	2[b]	3[c]	4	5	6[d]		7[e]
Orientation	Table parallel c-axis	Table perp. c-axis	Table perp. c-axis	Table perp. c-axis	Table parallel c-axis	Cut parallel c-axis		Cut perp. c-axis
Visual appearance	Dark red core, lighter red rim	Dark red core, lighter red rim	Dark red core, lighter red rim	Red core, lighter red rim	Dark red core, lighter red rim	Dark violet core, lighter red rim		Complex zoning dark violet core, light red rim
Number of scans	3	4	4	4	2	5	3	7
Number of analyses	109	138	138	138	78	208	108	288
Direction of scans	Perp. c-axis	Perp. c-axis	Perp. c-axis	Perp. c-axis	Perp. c-axis	Perp. c-axis	Parallel c-axis	Perp. c-axis
Analyses in wt.% (range)								
Al_2O_3	98.42–99.44	98.17–99.72	96.53–98.97	98.15–99.60	98.15–99.66	98.33–99.78	98.40–99.90	98.45–99.91
Cr_2O_3	0.26–0.89	0.42–1.05	0.90–2.86	0.60–0.89	0.39–0.98	0.40–1.03	0.42–0.69	0.40–1.34
V_2O_3	0.00–0.13	0.00–0.11	0.00–0.12	0.00–0.07	0.00–0.10	0.00–0.08	0.00–0.07	0.00–0.08
TiO_2	0.09–0.28	0.05–0.23	0.00–0.14	0.06–0.27	0.04–0.31	0.00–0.38	0.04–0.34	0.03–0.51
FeO	0.00–0.03	0.00–0.02	0.00–0.04	0.00–0.03	0.00–0.02	0.00–0.04	0.00–0.03	0.00–0.04
MnO	0.00–0.03	0.00–0.03	0.00–0.02	0.00–0.02	0.00–0.04	0.00–0.03	0.00–0.02	0.00–0.03
Chemical zoning	Cr	Cr and Ti	Cr	Cr	Cr and Ti	Ti/ Cr	No distinct zoning	Complex zoning of Cr and Ti
Area of high concentration	Core	Core	Core	Core	Core	Core/outer rim		
Correlation between Ti and Cr	No	Yes	No	No	Yes	No	No	No

[a] *All faceted samples had been heat treated; both rough samples were untreated. Perp. = perpendicular.*
[b] *See figure 28B.* [d] *See figure 28C*
[c] *See figure 28A.* [e] *see figure A-1.*

were found in this sample in a direction parallel to the c-axis.

In sample 7 (table 3), the complex growth and color zoning involving *c*, *n*, *r*, and *ω* faces (figure A-1) revealed an extremely complex zoning of both Cr_2O_3 and TiO_2 that does not fit any of the simple types described above.

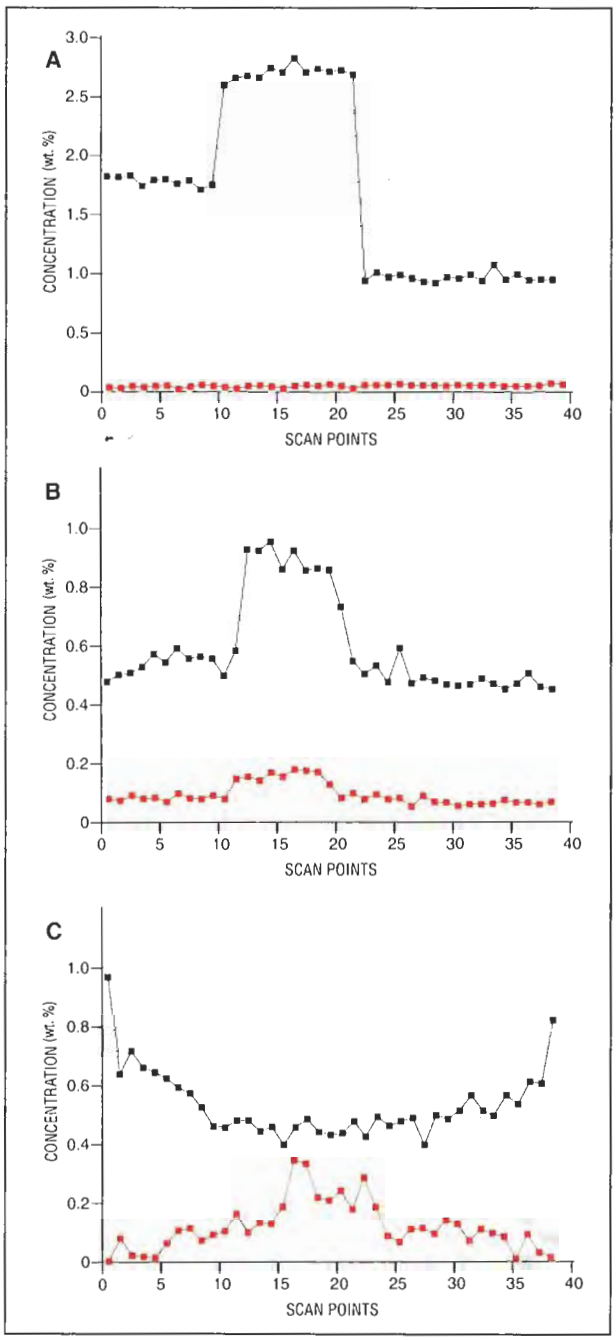

Figure 28. These three electron microprobe traverses reveal the differences in Cr_2O_3 contents (black squares) and TiO_2 contents (red squares) between core and rim areas of three Mong Hsu rubies. Samples A (no. 3, table 3) and B (no. 2, table 3) are both faceted and heat-treated; sample C (no. 6, table 3) is an untreated polished platelet. Sample A shows higher Cr_2O_3 in the core than the rim, and no TiO_2 zoning. Sample B shows Cr_2O_3 concentrations correlated with a distinct TiO_2 zoning, with higher Cr_2O_3 and TiO_2 contents in the core and lower values in the rim. Sample C reveals increased TiO_2 in the core, increasing Cr_2O_3 toward the outer zones of the rim, and an inverse correlation between Cr_2O_3 zoning and variations in TiO_2. All scans were performed in a direction perpendicular to the c-axis.

In some samples, we found a correlation between V_2O_3 and Cr_2O_3; that is, high chromium and relatively high vanadium in the intense red cores, with lower chromium and vanadium in the lighter red rims. No correlation was seen between iron and titanium or between iron and chromium.

Thus, it can be concluded that the color zoning correlates with a systematic variation in Cr_2O_3 and/or TiO_2 (see also box B): The violet (untreated) and intense red (heat-treated) cores of Mong Hsu rubies have significantly higher Cr_2O_3 concentrations than the lighter red "rim" layers around them. We also identified zones with high TiO_2 concentrations (relative to the rim portion) in the violet (untreated) and red (heat-treated) cores of some Mong Hsu rubies (type C). In some samples, we found both high Cr_2O_3 and high TiO_2 concentrations in the core.

In summary, it appears that the main chemical zoning of Mong Hsu rubies, between crystal core and rim zones, is due to greater amounts of chromium and/or titanium in the areas confined to the intense red or violet cores. Between distinct zones within the rims, chromium and/or titanium values also may vary (see box B, as well as figures 13 and 28C).

The trace-element concentrations of Mong Hsu rubies can be compared to those of natural rubies from other deposits of commercial importance, including Luc Yen (Vietnam), Morogoro (Tanzania), Mogok (Myanmar), Kenya, Sri Lanka, Malawi, and Thailand (Harder, 1969; Schmetzer, 1986b; Bank et al., 1988; Tang et al., 1988, 1989; Hänni and Schmetzer, 1991; Kane et al., 1991; Delé-Dubois et

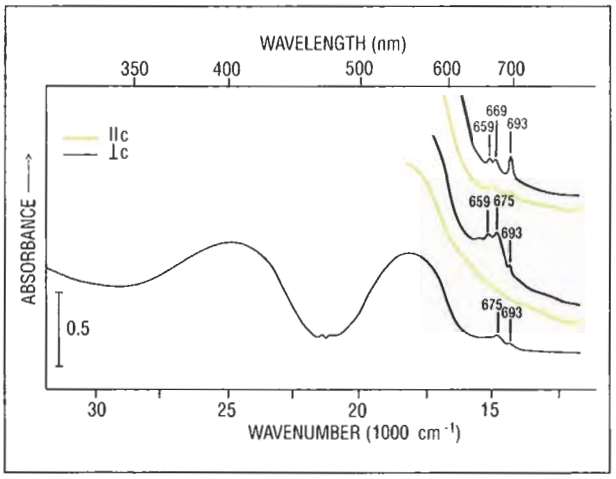

Figure 29. These absorption spectra were recorded in three Mong Hsu rubies. The top is from a heat-treated faceted stone with its table oriented parallel to the c-axis, 2.3 mm thick (sample 1, table 3). The middle is from the violet core of an untreated slice (about 2.5 mm thick) cut parallel to the c-axis (sample 6, table 3). The bottom is from an untreated slice (about 1 mm thick) cut perpendicular to the c-axis with violet core and red rim (see sample 7, table 3, figure A-1). In the red to yellow spectral range of untreated samples, a broad absorption without distinct maximum and an absorption band at 675 nm are superimposed on the chromium (ruby) spectrum.

al., 1993). The Cr_2O_3 concentrations in Mong Hsu rubies can be extremely high. The FeO concentrations are relatively low compared to those of rubies from other marble-type deposits such as Morogoro or Luc Yen. The upper end of the TiO_2 range is much higher than the values found in rubies from these same occurrences. The V_2O_3 concentrations are similar to those reported for rubies from Mogok, but can be much higher than those published for rubies from some other marble-type deposits, such as Morogoro and Luc Yen. The range of FeO, TiO_2 and V_2O_3 concentrations found in Mong Hsu rubies is different from those of rubies from basaltic rocks (e.g., Thailand).

The combination of relatively high Cr_2O_3, TiO_2, and V_2O_3 along with relatively low concentrations of FeO has so far not been reported for any of the various types of synthetic rubies (Tang et al., 1989; Muhlmeister and Devouard, 1991; Peretti and Smith, 1993; Hänni et al., 1994).

In summary, the trace-element patterns of Mong Hsu rubies are useful to distinguish faceted samples from their synthetic counterparts. Although there may be some overlaps with other natural rubies originating from marble deposits, trace-element contents of individual samples, in combination with other characteristics, can also be helpful for locality determination.

Spectroscopic Features. *Visible and Ultraviolet Spectroscopy.* Absorption spectra of heat-treated Mong Hsu rubies and of the outer rims of untreated specimens were typical of those seen in low-iron rubies, with no iron-related absorption at 450 nm. Absorption characteristics in the ultraviolet were similar to those of iron-poor rubies from marble-type deposits (Bosshart, 1982; Smith and Surdez, 1994).

The spectra of untreated samples with violet cores revealed additional absorption features in the red and yellow area, between about 800 nm and the broad chromium absorption band in the green range, which are superimposed on the ruby absorptions (figure 29). These absorption features are described as:

- a broad absorption in the spectrum parallel and perpendicular to the c-axis, ranging from about 800 nm to about 550 nm without a distinct absorption maximum, and
- a polarized absorption band in the spectrum perpendicular to the c-axis, with a maximum at 675 nm, that is, in the range of the well-known chromium lines at 693, 669, and 659 nm.

In different violet samples measured, the relative intensities of the bands in the red to yellow area vary. In some, the 675-nm band was weaker than the 693-nm Cr^{3+} absorption line; in others, the 675-nm absorption, which is strongly polarized, exceeded this well-known chromium absorption in intensity (figure 29).

These additional absorption features in the red, particularly the broad absorption, are responsible for the color in the cores, that is, light violet parallel to the c-axis and intense violet perpendicular to *c*. Thus, the violet color in Mong Hsu rubies is caused by the superimposition of a red (ruby) component caused by chromium and a blue component that is removed by heat treatment. The blue component consists of two different absorption features, which are more intense in the spectrum perpendicular to the c-axis.

Violet sapphires and purplish red rubies are known from various localities, such as Ratnapura, Sri Lanka, and Umba, Tanzania. In all types of violet samples from various occurrences, the blue

component of the violet color is due to a broad absorption band in the red area, which can be at least partially removed by heat treatment, even at relatively low temperatures such as 1000° or 1200°C, which have been used historically for the heat-treatment of corundum (Bauer and Schlossmacher, 1932).

An extremely broad absorption band in the red-to-green spectral region (between 800 and 500 nm) has been seen in blue sapphires from various localities and is generally assigned to an Fe^{2+}/Ti^{4+} charge-transfer absorption. The blue color in this type of low-iron sapphire (i.e., without a specific Fe^{2+}/Fe^{3+} absorption band in the near infrared) can also be partially removed by heat treatment at low temperatures; some of these sapphires turn colorless when heated (Schmetzer and Bank, 1980). If the iron-titanium charge-transfer absorption is superimposed on a ruby spectrum, the color of the sample is altered from red to purplish red, purple, or violet, according to the relative intensity of the two color-causing components in the spectrum (Schmetzer and Bank, 1981).

Given the spectral characteristics of Mong Hsu rubies and their titanium zoning, the additional broad absorption in the red and the resulting violet color of the cores of these rubies is consistent with the presence of such a blue sapphire component.

In the absorption spectrum of untreated Mong Hsu samples with violet cores, however, we also observed an additional polarized absorption band at 675 nm (figure 29), which is not fully understood at present. In some of the samples, this absorption band exceeded the 693-nm chromium line in intensity. The only correlation found in the literature for this band is an absorption in the spectrum of Mn^{4+} in corundum (Geschwind et al., 1962; Crozier, 1965; Potnau and Adde, 1976). Mn^{4+} appears in synthetic flux-grown and Verneuil-grown corundum crystals, which are doped by manganese, with MgO added for charge compensation. Mn^{4+} is isoelectronic with Cr^{3+} and has three d electrons. It reveals, in addition to the sharp 675-nm band, a broad absorption at about 470 nm and an absorption edge in the ultraviolet range, the low-energy tail of which extends to the visible area, causing an almost continuously increasing absorption from about 500 nm toward smaller wavelengths. If a broad absorption band of Mn^{4+} at 470 nm is present in the spectrum of chromium-bearing corundum, this absorption is, most probably, hidden between the two dominant color-causing chromium absorption bands. Thus, in a sample of Mong Hsu ruby with high amounts of chromium and relatively low manganese concentrations (see tables 2 and 3), it is conceivable that only the small 675-nm absorption band close to the small chromium fluorescence line at 693 nm will be observed. This assignment, however, needs further experimental research for confirmation, especially for the explanation of a possible stabilization mechanism by charge compensation and its reaction to heat-treatment.

In summary, the spectra of the violet cores in Mong Hsu rubies consist of the well-known absorption lines and absorption bands of Cr^{3+} in corundum, on which are superimposed a broad Fe^{2+}/Ti^{4+} charge-transfer absorption and an additional line at 675 nm, the nature of which is not yet known. The influence of one or both additional absorption features in the red on the violet color of different cores varies, and additional research is necessary (for example, by a combination of microscope absorption spectroscopy and microprobe analyses) to understand the cause of color in these highly zoned samples.

Infrared Spectroscopy. IR spectroscopy of transparent, heat-treated samples revealed spectra with sharp absorption lines in the 3000 to 3500 cm^{-1} range—either with two maxima, at 3233 and 3310 cm^{-1} (figure 30), or with one maximum at 3310 cm^{-1}—or spectra with a complete absence of infrared absorptions in the range mentioned. Smith and

Figure 30. This infrared spectrum of a heat-treated Mong Hsu ruby reveals sharp absorption lines at 3233 and 3310 cm^{-1}, which are assigned to OH-stretching vibrations. These lines are characteristic for OH groups in rubies, which are related to structural defects. Such lines are not found in flux-grown synthetic rubies.

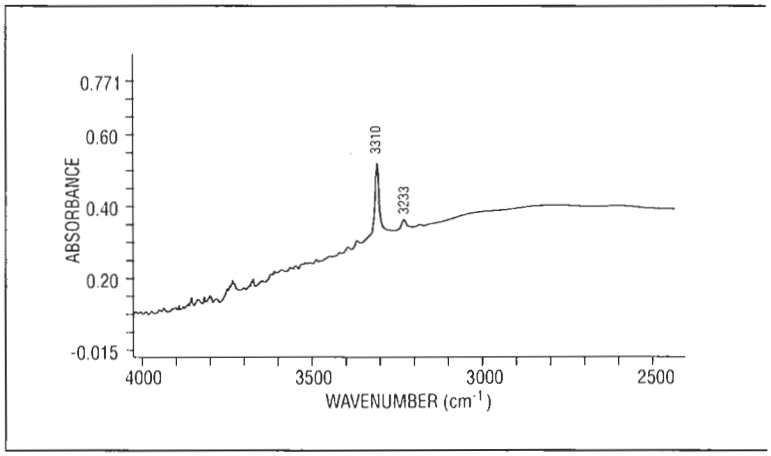

Surdez (1994) reported seven sharp bands of varying intensity at 3189 (weak), 3233 (medium), 3299 (very weak), 3310 (strong), 3368 (very weak), 3380 (very weak), and 3393 cm^{-1} (very weak) in the absorption spectra of Mong Hsu rubies. Similar features have been found in the infrared spectra of Verneuil-grown synthetic rubies and sapphires that were doped with various trace elements in different concentrations and, at least partly, annealed in a hydrogen atmosphere at high temperatures (Borer et al., 1970; Eigenmann and Günthard, 1971; Eigenmann et al., 1972; Blum et al., 1973; Volynets et al., 1972, 1974; Beran, 1991; Moon and Phillips, 1994). Consequently, the sharp absorption bands in the infrared spectra of Mong Hsu rubies are assigned to OH-stretching vibrations and indicate that hydroxyl groups have been incorporated in the crystal structure of some heat-treated samples.

Smith (1995) recorded an absorption spectrum in some untreated samples that consisted of several broad absorption bands. He assigned this spectrum to microscopic or submicroscopic inclusions of diaspore, AlO(OH).

OH-stretching vibrations were also measured previously in the infrared spectra of a few untreated ruby and sapphire samples from Sri Lanka (Schmetzer, unpublished), in a ruby from Sri Lanka and a blue sapphire from Montana (Beran, 1991), and in untreated blue Australian sapphires (Moon and Phillips, 1994). They were not found in the spectra of flux-grown synthetic rubies (Belt, 1967; Volynets et al., 1972; Peretti and Smith, 1994).

For practical gemology, the presence of OH-related absorption lines in the infrared spectrum of an unknown ruby indicates that the sample is not a flux-grown synthetic ruby, although it may be a Verneuil-grown or hydrothermally grown synthetic sample (either of which is more readily identifiable from natural rubies than the flux-grown material) or a natural stone. For discussion of the difference between Verneuil- and hydrothermally grown synthetic ruby, see Belt (1967), Beran (1991), and Peretti and Smith (1993, 1994).

SUMMARY AND CONCLUSION

Large quantities of rubies from the new deposit at Mong Hsu have been widely available since 1992. Most are heat-treated before they enter the jewelry trade. Mong Hsu rubies are easily recognized by their distinctive microscopic properties. They have a number of features that thus far have not been reported for rubies from other occurrences. These include:

- A distinct color zoning confined to specific growth structures, with one or two violet "cores" surrounded by a red "rim."
- Spectroscopic features in the red to yellow portion of the visible spectrum, with absorption bands that are removed during heat treatment to change the cores from violet to red.
- The presence of whitish particles in certain growth zones, formed as a result of heat treatment.

We found that the color zoning in our samples is closely related to a complex chemical zoning confined to growth layers formed parallel to the basal pinacoid, to the positive rhombohedron, and to two hexagonal dipyramids. We observed a distinct growth sequence whereby red and violet areas formed in various growth cycles, with a specific habit change between different growth zones. The variation in physical properties, such as refractive indices, is closely related to the chemical composition of the samples. Although those properties of the crystals that are related to different growth conditions during the formation of the rubies—that is, growth zoning, color zoning, and chemical zoning related to temperature and/or pressure and/or chemical composition of the environment—are well understood. Only preliminary models are presently available to provide a detailed explanation of the cause of successive growth cycles (Peretti and Mouawad, 1994).

Nor is there a comprehensive explanation for those properties of Mong Hsu rubies that change with heat treatment. Likewise, no model is available that can explain all features related to the change in UV-visible and IR spectroscopic properties, which are closely related to the color change and possibly also to the formation of the whitish particles.

The distinctive properties of Mong Hsu rubies are useful in separating faceted samples from their synthetic counterparts and also in establishing the locality of origin. The most prominent diagnostic properties of faceted, heat-treated Mong Hsu rubies require careful microscopic examination, using immersion techniques in conjunction with fiber-optic illumination. Key features include growth structures confined to a distinct color zoning between cores and rims; different types of whitish particles and whitish streamers are also of diagnostic value. Specialized laboratory techniques, such as XRF analysis and IR spectroscopy, provide additional diagnostic information. Problems for the trade

arise, however, from the large numbers of stones with fractures that appear to have been filled with a foreign material, especially partially healed fractures with glassy and/or crystalline fillers.

Acknowledgments: The authors are grateful to the following persons or companies who kindly submitted Mong Hsu rubies for the present investigation: Mouawad Bangkok Co., Bangkok, Thailand; H. Ho, Asian Institute of Gemmological Sciences (AIGS), Bangkok; Myanma Gems Enterprise, Yangon, Myanmar; R. Kunkongkaphan, Mandalay Co., Mae Sai, Thailand; J. Belmont, K. V. Gems Co., Bangkok; Dr. H.A. Hänni, SSEF (Basel) and University of Basel, Switzerland; R. E. Kane, Helena, Montana; H. M. Graf, Grafgem, Winterthur, Switzerland; and R. Bieler, Ernst Färber Company, Munich, Germany. For technical assistance, we are grateful to C. P. Smith, Gübelin Gemmological Laboratory, Lucerne, Switzerland (infrared spectroscopy); Prof. Dr. W. Stern, Geochemical Laboratory, University of Basel, Switzerland (XRF-analysis); Dr. J. Dubessy, CREGU, Vandoeuvre-Les-Nancy, France (Raman spectroscopy); Prof. Dr. R. Guggenheim and M. Düggelin, Institute of Geology, University of Basel, Switzerland (electron microscopy); and Prof. Dr. E. Gübelin, Lucerne, Switzerland (photomicrography).

REFERENCES

Bank H., Henn U., Lind Th. (1988) Rubine aus Malawi. *Zeitschrift der Deutschen Gemmologischen Gesellschaft*, Vol. 37, No. 3/4, pp. 113–119.

Bauer M., Schlossmacher K. (1932) *Edelsteinkunde. 3. Aufl.*, Bernhard Tauchnitz, Leipzig, p. 209, 498.

Belt R.F. (1967) Hydrothermal ruby: Infrared spectra and X-ray topography. *Journal of Applied Physics*, Vol. 38, No. 6, pp. 2688–2689.

Beran A. (1991) Trace hydrogen in Verneuil-grown corundum and its color varieties—An IR spectroscopic study. *European Journal of Mineralogy*, Vol. 3, pp. 971–975.

Blum H., Frey R., Günthard Hs.H., Ha Tae-Kyu (1973) Ab initio scf study of OHO^{3-} system and its relation to the structure of alpha-Al_2O_3:OHO^{3-}(Me^{2+}). *Chemical Physics*, Vol. 2, pp. 262–270.

Borer W.J., Günthard Hs.H., Ballmer P. (1970) Solid state reactions and defects in Verneuil laser rubies. *Helvetica Physica Acta*, Vol. 43, pp. 74–92.

Bosshart G. (1982) Distinction of natural and synthetic rubies by ultraviolet spectrophotometry. *Journal of Gemmology*, Vol. 18, No. 2, pp. 145–160.

Burma's Mongshu mine rediscovered, heat-treated rubies comparable to Mogok quality (1993). *Jewelry Newsline*, Vol. 1, No. 2, p. 1, 8.

Clark C. (1993) Thai cooking class. *JewelSiam*, Vol. 4, No. 5, p. 57.

Crozier M.H. (1965) Optical Zeeman effect in the R_1 and R_2 lines of Mn^{4+} in Al_2O_3. *Physics Letters*, Vol. 18, No. 3, pp. 219–220.

Delé-Dubois M.L., Fournier J., Peretti A. (1993) Rubis du Vietnam—Etude comparative avec les rubis de Birmanie et d'autres provenances. *Revue de Gemmologie a.f.g.*, No. 114, March 1993, pp. 7–10.

Earth Sciences Research Division (1977) Geological Map of the Socialist Republic of the Union of Myanmar 1:1'000'000, with brochure, 22 pp.

Eigenmann K., Günthard Hs.H. (1971) Hydrogen incorporation in doped alpha-Al_2O_3 by high temperature redox reactions. *Chemical Physics Letters*, Vol. 12, No. 1, pp. 12–15.

Eigenmann K., Kurtz K., Günthard Hs.H. (1972) Solid state reactions and defects in doped Verneuil sapphire. *Helvetica Physica Acta*, Vol. 45, pp. 452–480.

Geschwind S., Kisliuk P., Klein M.P., Remeika J.P., Wood D.L. (1962) Sharp-line fluorescence, electron paramagnetic resonance, and thermoluminescence of Mn^{4+} in alpha-Al_2O_3. *Physical Review*, Vol. 126, No. 5, pp. 1684–1686.

Glass filled rubies increasing (1994). *Jewellery News Asia*, No. 119, July, pp. 66, 68, 70.

Hänni H.A. (1986) Behandelte Korunde mit glasartigen Füllungen. *Zeitschrift der Deutschen Gemmologischen Gesellschaft*, Vol. 35, No. 3/4, pp. 87–96.

Hänni H.A. (1992) Identification of fissure-treated gemstones. *Journal of Gemmology*, Vol. 23, No. 4, pp. 201–205.

Hänni H.A., Schmetzer K. (1991) New rubies from the Morogoro area, Tanzania. *Gems & Gemology*, Vol. 27, No. 3, pp. 156–167.

Hänni H.A., Schmetzer K., Bernhardt H.-J. (1994) Synthetic rubies by Douros: A new challenge for gemologists. *Gems & Gemology*, Vol. 30, No. 2, pp. 72–86.

Harder H. (1969) Farbgebende Spurenelemente in natürlichen Korunden. *Neues Jahrbuch für Mineralogie Abhandlungen*, Vol. 110, pp. 128–141.

Henn U., Bank H. (1993) Neues Rubinvorkommen in Myanmar (Burma). *Zeitschrift der Deutschen Gemmologischen Gesellschaft*, Vol. 42, No. 2/3, pp. 63–65.

Hlaing U Tin (1981) Mineralogical studies and minor element analyses of corundum and associated minerals of the Mogok gemstone tract. M.S. thesis, University of Rangoon, Myanmar, 217 pp.

Hlaing U Tin (1991) A new Myanmar ruby deposit. *Australian Gemmologist*, Vol. 17, No. 12, pp. 509–510.

Hlaing U Tin (1993) Mong Hsu ruby update. *Australian Gemmologist*, Vol. 18, No. 5, pp. 157–160.

Hlaing U Tin (1994) A trip to Mong Hsu. *JewelSiam*, Vol. 5, No. 1, pp. 54–57.

Hughes R.W. (1988) Surface repaired corundum—Two unusual variations. *Journal of Gemmology*, Vol. 21, No. 1, pp. 8–10.

Hunstiger C. (1990) Darstellung und Vergleich primärer Rubinvorkommen in metamorphen Muttergesteinen. Petrographie und Phasenpetrologie. Teil III. *Zeitschrift der Deutschen Gemmologischen Gesellschaft*, Vol. 39, No. 2/3, pp. 121–145.

Jobbins E.A. (1992) A taste of new gem deposits in South East Asia. *Gems and Jewellery News*, Vol. 2, No. 1, p. 12.

Kammerling R.C., Scarratt K., Bosshart G., Jobbins E.A., Kane R.E., Gübelin E.J., Levinson A.A. (1994) Myanmar and its gems—An update. *Journal of Gemmology*, Vol. 24, No. 1, pp. 3–40.

Kane R.E. (1984) Natural rubies with glass-filled cavities. *Gems & Gemology*, Vol. 20, No. 4, pp. 187–199.

Kane R.E., Kammerling R.C. (1992) Status of ruby and sapphire mining in the Mogok stone tract. *Gems & Gemology*, Vol. 28, No. 3, pp. 152–174.

Kane R.E., McClure S.F., Kammerling R.C., Nguyen Dang Khoa, Mora C., Repetto S., Nguyen Duc Khai, Koivula J.I. (1991): Rubies and fancy sapphires from Vietnam. *Gems & Gemology*, Vol. 27, No. 3, pp. 136–155.

Keller P.C. (1983) The rubies of Burma: A review of the Mogok stone tract. *Gems & Gemology*, Vol. 19, No. 4, pp. 209–219.

Kiefert L., Schmetzer K. (1991) The microscopic determination of structural properties for the characterization of optical uniaxial natural and synthetic gemstones, part 1: General considerations and description of the methods. *Journal of Gemmology*, Vol. 22, No. 6, pp. 344–354.

Koivula J.I., Kammerling R.C., Fritsch E. (1993a) Gem news: Update on ruby enhancement. *Gems & Gemology*, Vol. 29, No. 3, pp. 214–215.

Koivula J.I., Kammerling R.C., Fritsch E. (1993b) Gem news: Update on Monghsu ruby. *Gems & Gemology*, Vol. 29, No. 4, pp. 286–287.

Laughter T.L. (1993a) Mong Hsu mix-up. *JewelSiam*, Vol. 4, No. 5, pp. 34–37.

Laughter T.L. (1993b) How do you do? I am from Mong Hsu. *JewelSiam*, Vol. 4, No. 5, pp. 38–41.

Milisenda C.C., Henn U. (1994) Neues Rubinvorkommen in Myanmar (Burma). *Goldschmiede und Uhrmacher Zeitung*, Vol. 92, No. 4, pp. 147–148.

Moon A.R., Phillips M.R. (1994) Defect clustering and color in Fe,Ti:alpha-Al_2O_3. *Journal of the American Ceramic Society*, Vol. 77, No. 2, pp. 356–367.

Muhlmeister S., Devouard B. (1991) Determining the natural or synthetic origin of rubies using energy-dispersive X-ray fluorescence (EDXRF). In A.S. Keller, Ed., *Proceedings of the International Gemological Symposium 1991*, Gemological Institute of America, Santa Monica, CA, pp. 139–140.

Peretti A. (1993) Foreign substances in Mong Hsu rubies. *JewelSiam*, Vol. 4, No. 5, p. 42.

Peretti A., Smith C.P. (1993) A new type of synthetic ruby on the market: offered as hydrothermal rubies from Novosibirsk. *Australian Gemmologist*, Vol. 18, No. 5, pp. 149–157.

Peretti A., Smith C.P. (1994) Letter to the editor. *Journal of Gemmology*, Vol. 24, No. 1, pp. 61–63.

Peretti A., Mouawad F. (1994) Fluorite inclusions in Mong Hsu ruby. *JewelSiam*, Vol. 5, No. 4, pp. 136–137.

Potnau J., Adde R. (1976) Crystalline field parameters of Cr^{2+} and Cr^{4+} in corundum. *Journal de Physique*, Vol. 37, pp. 603–610.

Prieto A.C., Dubessy J., Cathelineau M. (1991) Structure-composition relationships in trioctahedral chlorites: A vibrational spectroscopy study. *Clays and Clay Minerals*, Vol. 39, No. 5, pp. 531–539.

Rains wash out Mong Hsu supply (1994). *JewelSiam*, Vol. 5, No. 5, p. 78.

Scarratt K., Harding R.R. (1984) Glass infilling of cavities in natural ruby. *Journal of Gemmology*, Vol. 19, No. 4, pp. 293–297.

Scarratt K., Harding R.R., Din V.K. (1986) Glass fillings in sapphire. *Journal of Gemmology*, Vol. 20, No. 4, pp. 203–207.

Schmetzer K. (1986a) An improved sample holder and its use in the distinction of natural and synthetic ruby as well as natural and synthetic amethyst. *Journal of Gemmology*, Vol. 20, No. 1, pp. 20–33.

Schmetzer K. (1986b) *Natürliche und synthetische Rubine—Eigenschaften und Bestimmung*. Stuttgart, Schweizerbart.

Schmetzer K., Bank H. (1980) Explanations of the absorption spectra of natural and synthetic Fe- and Ti-containing corundums. *Neues Jahrbuch für Mineralogie Abhandlungen*, Vol. 139, No. 2, pp. 216–225.

Schmetzer K., Bank H. (1981) The color of natural corundum. *Neues Jahrbuch für Mineralogie Monatshefte*, Vol. 1981, No. 2, pp. 59–68.

Smith C.P. (1995) A contribution to understanding the infrared spectra of Mong Hsu rubies. *Journal of Gemmology*, Vol. 24, No. 5, pp. 321–335.

Smith C.P., Surdez N. (1994) The Mong Hsu ruby: a new type of Burmese ruby. *JewelSiam*, Vol. 4, No. 6, pp. 82–98.

Special report: Mong Hsu ruby fact sheet (1993). *JewelSiam*, Vol. 4, No. 5, p. 33.

Tang S.M., Tang S.H., Tang, T.S., Retty A.T. (1988) Analysis of Burmese and Thai rubies by PIXE. *Applied Spectroscopy*, Vol. 42, No. 1, pp. 44–48.

Tang S.M., Tang S.H., Mok K.F., Retty A.T., Tay T.S. (1989) A study of natural and synthetic rubies by PIXE. *Applied Spectroscopy*, Vol. 43, No. 2, pp. 219–223.

Volynets F.K., Sidorova E.A., Stsepuro N.A. (1974) OH groups in corundum crystals which were grown with the Verneille technique. *Journal of Applied Spectroscopy*, Vol. 17, pp. 1626–1628.

Volynets F.K., Vorob'ev V.G., Sidorova E.A. (1972) Infrared absorption bands in corundum crystals. *Journal of Applied Spectroscopy*, Vol. 10, pp. 665–667.